June 22, 2023

Defining dark jets at the particle level

Gustav Lindberg

Department of Physics, Division of Particle Physics, Lund University

Masters thesis supervised by Dag Gillberg, Caterina Doglioni and Sukanya Sinha

LUND
UNIVERSITY

Popular Science Description

Almost all phenomena we have studied in our universe can be explained by four forces, namely: electromagnetism, gravity, the weak force and the strong force. The latter force is of most relevance for the work presented in this thesis. The strong force, also called quantum chromodynamics or QCD, binds elementary particles called quarks together into so-called hadrons. The most common types of hadrons in nature are protons and neutrons, present in atomic nuclei, which are baryons meaning they contain three quarks. Another type of hadrons are mesons, which are made up of a quark and an antiquark. Quarks can only exist inside of hadrons, which means that attempting to knock a quark out of a hadron will produce an entire group of new hadrons called a jet.

However, some things remain unexplained, such as dark matter. This is matter that has not been observed but is still known to exist and have mass because of the gravitational force it exerts on stars and galaxies. Dark matter is one of the greatest mysteries in physics since we know almost nothing about it. This, together with other unexplained phenomena, seems to be an indication that there are more particles than those observed so far.

One hypothesis that could explain dark matter is called dark QCD, and suggests that there would be particles called dark quarks, which do not interact with everyday matter, but interact with themselves through a force similar to the strong force. Dark quarks would then be grouped together into dark hadrons, of which some would be dark matter candidates, and can be knocked out of dark hadrons and produce dark jets.

At CERN in Switzerland, there is a particle accelerator called the LHC, which has the goal to discover new particles and interactions. It has been successful in discovering the Higgs boson, which explains why particles have mass, but has so far not been able to observe dark matter. If dark QCD is true, it is however possible that dark jets are produced at the LHC but are difficult to detect.

My work focus on such dark jets, and I am making a first, generic proposal for a technical definition for a dark jet, that is suitable both for theoretical and experimental physicists. This definition can be used as a middle ground between theorists and experimentalists, for example so that theorists can more easily check if a certain dark QCD model is already excluded by experiments. It will also allow theorists to get a better idea of the experimental signature of each model, which will inform experimentalists what to look for.

Abstract

One hypothesis that attempts to explain dark matter is dark QCD, which suggests that there would be a dark sector made up of dark quarks. Dark quarks would interact with each other through dark QCD similar to how Standard Model quarks interact with each other through Standard Model QCD. Dark QCD would have several QCD-like features, one of which is dark jets. If dark quarks are produced at the LHC, they would produce dark jets, which could potentially have prompt or displaced decays into Standard Model jets, either fully or partially. However, there is currently no standardized definition of which jets should be considered dark. In this thesis, we will propose such a definition at particle level, and we will test the proposed definition on several dark QCD models. This definition is intended to be able to be used on a wide range of theoretical models, and can be refined to target specific models. We find that a suitable baseline definition of a dark jet is a jet for which at least 80% of its p_{T} originates from dark particles.

Contents

1 Introduction **1**

2 Theory **3**

2.1 The Standard Model . . . 3

2.1.1 The SU(2) group, spin and symmetry breaking . . . 4

2.1.2 The SU(3) group: a mathematical model for QCD . . . 7

2.1.3 Color confinement and jets . . . 9

2.1.4 Types of hadrons . . . 11

2.2 Dark QCD . . . 13

2.2.1 Parameters of dark QCD . . . 13

2.2.2 Dark matter portals . . . 15

2.2.3 Dark QCD models . . . 17

3 LHC physics **21**

3.1 Physics of proton-proton collisions . . . 21

3.1.1 Parton, particle and reconstruction level . . . 21

3.1.2 Observable particles . . . 23

3.1.3 Coordinate system . . . 23

3.1.4 Jet algorithms . . . 25

3.2 Experimental setup of the LHC . . . 26

3.2.1 The LHC accelerator . . . 26

3.2.2 Principle of a multi-purpose particle detector . . . 27

4 Analysis **29**

4.1 Methodology . . . 29

4.1.1 Monte Carlo samples . . . 29

4.1.2 Analysis tools . . . 29

4.2 Initial dark jet studies . . . 29

4.3 Choice of jet algorithm parameters . . . 31

4.3.1 Input particles to jet building . . . 32

4.3.2 Choice of jet radius . . . 33

4.4 Proposed dark jet definition . . . 36

4.4.1 Motivation . . . 36

4.4.2 Definition . . . 39

4.5 Validation of the proposed dark jet definition . . . 41

4.5.1 Jet multiplicity . . . 41

4.5.2 Dijet invariant mass 43
4.6 Suggestions for experimental analyses 44
4.6.1 Invisibility 44
4.6.2 Lepton fraction 46
4.6.3 Dijet invariant mass 47
4.6.4 Event shape observables 48

5 Conclusion **50**

References **51**

1 Introduction

Most of how the universe works can be explained with just a limited number of particle fields that interact with each other. These particle fields constitute the *Standard Model of particle physics*. One type of particle in the Standard Model is called *quarks*. Free quarks are never found in nature, instead they are grouped together into *hadrons*. In nature, the most common types of hadrons are protons and neutrons, which make up atomic nuclei.

Quarks are bound very tightly together in hadrons. However, with sufficient energy, it is possible to knock out quarks. When this happens, additional quark-antiquark pairs will be produced so that the quarks are always inside hadrons. This means that if a very heavy particle produced at the LHC decays into quarks, the quarks will have enough energy to produce many of these quark-antiquark pairs, which will result in many collimated hadrons reaching the detector. These collimated groups of hadrons are called *jets*. How and why jets are produced will be explained in more detail in section 2.1.3.

While the Standard Model is successful at explaining most of what we can observe, there are some things that it cannot explain. One of those things is *dark matter*, which is matter that we know exists due to astrophysical evidence but that we cannot see directly.

The existence of dark matter was first suggested in the 1930s, when several astronomers calculated the mass of galaxies based on gravitational effects, and saw that this mass was significantly larger than what would be expected based on what was visible [1]. At the time, they did not think that dark matter was a new type of matter, but rather ordinary matter that was too dim to be visible. However, we know today that dark matter cannot be made of Standard Model particles, otherwise heavier elements would have been created during big bang nucleosynthesis [2]. We also know that dark matter must be electrically neutral, otherwise it would have interacted with ordinary matter in ways that we would have detected.

However, while there are a few constraints on what dark matter cannot be, we still have very little understanding of what it is. There are many widely varying hypotheses on what properties dark particles might have. Some of these, such as weakly interacting massive particles, suggest that dark matter consists of very heavy particles [3], while others, such as axions, assume that dark matter is made of of very light particles [4]. Some hypotheses suggest that there are many new particles and interactions which form a *dark sector*, among which one or several particles can be dark matter candidates [2].

One dark sector hypothesis is *dark QCD*, which suggests that dark particles could behave similarly to Standard Model quarks, in the sense that there would be *dark quarks* that are grouped together into *dark hadrons*. This does not mean that dark particles would interact through the Standard Model strong force, but rather that the dark sector would be a copy of Standard Model quarks and gluons that does not interact with the Standard Model directly. Dark QCD is the dark matter hypothesis that will be studied in this thesis. Dark QCD includes a wide range of specific models, and a number of examples will be studied in this thesis.

Since dark QCD is assumed to behave similarly to Standard Model QCD, this means that dark jets can be produced if two dark quarks are knocked out at very high energies, which could for example happen at the LHC if a heavy boson that interacts with both Standard Model quarks and dark quarks decays into a dark quark-antiquark pair. This means that evidence for dark QCD can be searched for at the LHC by searching for dark jets.

While dark jets have been studied before [5], there is no standardized definition of whether a given jet should be considered dark. This is non-trivial since background particles originating from Standard Model processes may reach the detector in the same region as the dark jet, resulting in jets that are not "entirely dark".

In this thesis, we will propose a technical definition of dark jets that is useful both for the theoretical

and experimental communities. It should therefore be made at the so-called particle level, which loosely corresponds to "what a perfect detector would see". The particle level is an established standard in particle physics as the intersection between theory and experiment, and is therefore an appropriate choice for the dark jet definition.

First, some theoretical and experimental background will be given, which can provide a better understanding of our analysis. We then run some preliminary analyses at particle level, which allow us to come up with a proposed definition. We then test this definition by looking at different dark QCD models and check if quantities related to dark jets behave as expected, as we want the definition to be suitable for any dark sector model. Finally, we look at the expected experimental signature, to try to find observables that are typical for dark jets in different models.

2 Theory

In this section, we first go through some theoretical aspects of the Standard Model, especially QCD. We then look more closely at how different dark QCD models work.

2.1 The Standard Model

As we can see in Figure 2.1, the Standard Model is made up of two types of particles: fermions, which have half integer spin, and bosons, which have integer spin.

The bosons are composed of

- *photons*, which mediate the electromagnetic force,
- *gluons*, which mediate the strong force,
- *W and Z bosons*, which mediate the weak force, and
- the *Higgs boson*, which is needed for most particles to have mass in the Standard Model.

Fermions can be divided into two categories, *quarks* and *leptons*. Quarks make up composite particles called hadrons. The two only hadrons that can be found in stable particles are protons and neutrons, which make up atomic nuclei. Since neutrons are only stable inside atomic nuclei and free neutrons are unstable, the only hadron that is stable on its own is the proton. The only leptons that are found in atoms are electrons. Neutrinos, while stable, have no electric charge so they rarely interact with matter, and the muon and tau lepton are unstable.

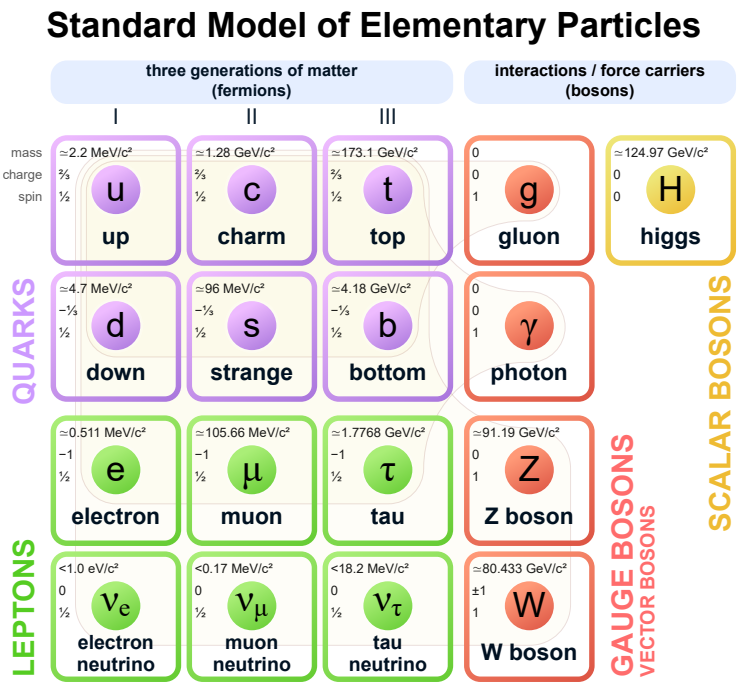

Figure 2.1: Particles in the Standard Model. Source: Wikipedia

2.1.1 The SU(2) group, spin and symmetry breaking

The Standard Model has several symmetries, which can be described mathematically by groups. The groups that describe the Standard Model are the SU(n) groups of matrices, where $n \in \mathbb{N}^*$. Formally, the SU(n) group is defined as the group of $n \times n$ complex matrices with determinant 1 such that their inverse is equal to their Hermitian conjugate:

$$\mathrm{SU}(n) = \{A \in \mathbb{C}^{n\times n} | \det(A) = 1, A^{-1} = A^\dagger\}. \tag{2.1}$$

One can prove that matrices in SU(n) can be parametrized using $n^2 - 1$ real parameters $x_1, \ldots, x_{n^2-1}$. This means that any matrix $A \in \mathrm{SU}(n)$ can be written as the result of a continuous function $A(x_1, \ldots, x_{n^2-1})$, where $A(0, \ldots, 0) = I$. Using this, we can form so-called generator matrices $g_1, \ldots, g_{n^2-1}$ of SU(n):

$$g_i = \frac{\partial}{\partial x_i} A(x_1, \ldots, x_{n^2-1})\bigg|_{x_1=\cdots=x_{n^2-1}=0}. \tag{2.2}$$

The generator matrices can be seen as the first order terms of the Taylor expansion of the group around the identity matrix.

For SU(2), the generating matrices are the *Pauli matrices* $\sigma_1, \sigma_2, \sigma_3$:

$$\sigma_1 = \begin{pmatrix} 0 & 1 \\ 1 & 0 \end{pmatrix} \qquad \sigma_2 = \begin{pmatrix} 0 & -i \\ i & 0 \end{pmatrix} \qquad \sigma_3 = \begin{pmatrix} 1 & 0 \\ 0 & -1 \end{pmatrix}. \tag{2.3}$$

One of the quantities that can be described by SU(2) is *spin*. Fermions, which have spin $\frac{1}{2}$, have two possible spin states: spin up $|\uparrow\rangle$ and spin down $|\downarrow\rangle$. This means that fermions form an SU(2) *doublet* under spin. These states can be written as vectors:

$$|\uparrow\rangle = \begin{pmatrix} 1 \\ 0 \end{pmatrix} \qquad |\downarrow\rangle = \begin{pmatrix} 0 \\ 1 \end{pmatrix}. \tag{2.4}$$

When acting on these vectors with an arbitrary matrix in SU(2), the result will still be a physical state (which in general can be a superposition state of $|\uparrow\rangle$ and $|\downarrow\rangle$, potentially with a complex phase). This means that the Standard Model is symmetric under spin SU(2).

The Pauli matrices can be combined into ladder operators that act on these vectors:

$$\hat{S}_+ = \frac{1}{2}(\sigma_1 + i\sigma_2) \qquad \hat{S}_- = \frac{1}{2}(\sigma_1 - i\sigma_2) \qquad \hat{S}_z = \frac{1}{2}\sigma_3. \tag{2.5}$$

It is easy to prove that $|\uparrow\rangle$ and $|\downarrow\rangle$ are the eigenstates of $\hat{S}_z$, with eigenvalues $+\frac{1}{2}$ and $-\frac{1}{2}$, respectively. These eigenvalues are commonly denoted s_z, which means that spin up fermions have $s_z = +\frac{1}{2}$ and spin down fermions have $s_z = -\frac{1}{2}$. This means that the $\hat{S}_z$ operator can be used to "measure" the spin s_z, since

$$\hat{S}_z |\psi\rangle = s_z |\psi\rangle \tag{2.6}$$

for any spin eigenstate $|\psi\rangle$.

It is also easy to prove that acting with $\hat{S}_+$ on a spin down state returns a spin up state (so $\hat{S}_+$ "raises" the spin), and acting with $\hat{S}_-$ on a spin up state returns a spin down state (so $\hat{S}_-$ "lowers" the spin):

$$\hat{S}_+ |\downarrow\rangle \propto |\uparrow\rangle \qquad \hat{S}_- |\uparrow\rangle \propto |\downarrow\rangle. \tag{2.7}$$

If one tries to raise the spin of a spin up state or lower the spin of a spin down state, the result is zero:

$$\hat{S}_+ |\uparrow\rangle = \hat{S}_- |\downarrow\rangle = 0. \tag{2.8}$$

The spin can be seen as a 3-vector with an operator $\hat{\vec{S}}$ defined as

$$\hat{\vec{S}} = \frac{1}{2}(\sigma_1, \sigma_2, \sigma_3). \tag{2.9}$$

This means that $\hat{S}_z$ is the z-component of $\hat{\vec{S}}$. Since the three Pauli matrices do not commute, they do not have common eigenvalues, so it is not possible to measure the three components of the spin vector simultaneously. Choosing to measure the spin along the z-axis is just a convention, the physics would have been the same if we would have measured along any other axes by swapping the Pauli matrices in equation (2.5).

It is also possible to measure the magnitude of the spin vector by defining the $\hat{S}^2$ operator:

$$\hat{S}^2 = \hat{\vec{S}} \cdot \hat{\vec{S}}. \tag{2.10}$$

This operator relates to the magnitude s of the spin vector as

$$\hat{S}^2 \left|\psi\right\rangle = s(s+1) \left|\psi\right\rangle. \tag{2.11}$$

Since $\hat{S}^2$ commutes with all the Pauli matrices, they have common eigenstates. Fermions are always in an eigenstate with $s = \frac{1}{2}$, vector bosons are always in an eigenstate with $s = 1$ and scalar bosons are always in an eigenstate with $s = 0$.

Two-particle states can be obtained by taking the tensor product of single-particle states. If we take two fermions in spin eigenstates and combine them into two-particle states, there are four possible states:

$$\left|\uparrow\uparrow\right\rangle = \begin{pmatrix}1\\0\\0\\0\end{pmatrix} \qquad \left|\uparrow\downarrow\right\rangle = \begin{pmatrix}0\\1\\0\\0\end{pmatrix} \qquad \left|\downarrow\uparrow\right\rangle = \begin{pmatrix}0\\0\\1\\0\end{pmatrix} \qquad \left|\downarrow\downarrow\right\rangle = \begin{pmatrix}0\\0\\0\\1\end{pmatrix}. \tag{2.12}$$

These can be obtained from the states in equation (2.4) by taking the tensor product: for example, $\left|\uparrow\uparrow\right\rangle = \left|\uparrow\right\rangle \otimes \left|\uparrow\right\rangle$.

The operators $\hat{S}_+$, $\hat{S}_x$, $\hat{S}_y$ and $\hat{S}_z$ for the two-particle states can be obtained by taking the tensor product with the 2×2 identity matrix in the following way:

$$(\hat{S}_z)_4 = (\hat{S}_z)_2 \otimes I_2 + I_2 \otimes (\hat{S}_z)_2, \tag{2.13}$$

and the same for the other operators. $(\hat{S}_z)_4$ is a 4×4 matrix acting on the two particle states, and $(\hat{S}_z)_2$ is the 2×2 matrix acting on single particle states that we saw earlier. This works because the first term in equation (2.13) measures the s_z of the first particle, and the second term measures the s_z of the second particle, and s_z is additive. This process does however not work for $\hat{S}^2$, since it is not additive. To get the two-particle version of $\hat{S}^2$ we need to use $\hat{S}^2 = \hat{\vec{S}} \cdot \hat{\vec{S}}$, where $\hat{\vec{S}}$ is the vector of the two-particle versions of $\hat{S}_x$, $\hat{S}_y$ and $\hat{S}_z$.

It is easy to prove that $\hat{S}_z \left|\uparrow\uparrow\right\rangle = 1 \left|\uparrow\uparrow\right\rangle$, $\hat{S}_z \left|\downarrow\downarrow\right\rangle = -1 \left|\downarrow\downarrow\right\rangle$ and $\hat{S}_z \left|\uparrow\downarrow\right\rangle = \hat{S}_z \left|\downarrow\uparrow\right\rangle = 0$. We can also lower the spin of the $\left|\uparrow\uparrow\right\rangle$ state by applying $\hat{S}_-$. If we do so, we get

$$\hat{S}_- \left|\uparrow\uparrow\right\rangle \propto \frac{1}{\sqrt{2}}(\left|\uparrow\downarrow\right\rangle + \left|\downarrow\uparrow\right\rangle). \tag{2.14}$$

This means that the $\frac{1}{\sqrt{2}}(\left|\uparrow\downarrow\right\rangle + \left|\downarrow\uparrow\right\rangle)$ is a spin-1 state with $s_z = 0$. This can be confirmed by applying $\hat{S}^2$:

$$\hat{S}^2 \frac{1}{\sqrt{2}}(\left|\uparrow\downarrow\right\rangle + \left|\downarrow\uparrow\right\rangle) = 1(1+1)\frac{1}{\sqrt{2}}(\left|\uparrow\downarrow\right\rangle + \left|\downarrow\uparrow\right\rangle). \tag{2.15}$$

Comparing this with equation (2.11) shows us that this state has $s = 1$. This means that even though this state has $s_z = 0$, it is still a spin-1 state.

So spin-1 states can have three possible values of s_z: $+1$, 0 or -1. This forms an SU(2) *triplet*.

The state that is orthogonal to this is $\frac{1}{\sqrt{2}}(|\uparrow\downarrow\rangle - |\downarrow\uparrow\rangle)$. It is straightforward to prove that acting on this state with $\hat{S}^2$ gives zero (which is equal to $0(0+1)$), which means that this state has $s = 0$. So this is a spin-0 state, and since there is only one such state it is called an SU(2) *singlet*.

The behavior of bosons with respect to spin is the same as two-fermion states: vector bosons have spin 1 and can therefore have three spin states, and scalar bosons have spin 0 and can therefore only have one spin state.

If we look at the fermions in Figure 2.1, we notice that each fermion comes in two versions: one with a higher electric charge and one with a lower electric charge. For example, the up quark and the down quark are both first generation quarks, with the only difference that one has charge $+\frac{2}{3}$ and one has charge $-\frac{1}{3}$. This symmetry can also be described by SU(2), but not by spin, since each fermion can have spin up or spin down regardless of what type of particle it is. This SU(2) symmetry is a different one, which is called *weak isospin*. This means that the up quark and the down quark are two weak isospin states of the first generation quark, with the up quark having weak isospin up and the down quark having weak isospin down. The same is true for the higher generation quarks and for the leptons (for instance the electron has weak isospin down and the electron neutrino has weak isospin up). Just like spin eigenstates have an s_z eigenvalue, weak isospin states have an eigenvalue, which we call w_z. This means that particles with weak isospin up (up-type quarks and neutrinos) have $w_z = +\frac{1}{2}$, and particles with weak isospin down (down-type quarks and charged leptons) have $w_z = -\frac{1}{2}$. Antiparticles have the opposite weak isospin compared to the corresponding particles. Note however that this is only true for left-handed fermions: right-handed fermions are weak isospin singlets with $w_z = 0$.

Some bosons also have weak isospin. The W bosons form a triplet under weak isospin: the W^+ boson has $w_z = +1$, and the W^- boson has $w_z = -1$. The particle in this triplet with $w_z = 0$ is called the W^0 boson, however it is not a mass eigenstate so it is not physical.

The gluon is a singlet state under weak isospin, meaning it has weak isospin zero. There is another weak isospin singlet boson called the B boson, however, just like the W^0 boson, the B boson is not a mass eigenstate. There are however two superposition states of the B and W^0 that are mass eigenstates: these are the photon and the Z boson.

Unlike spin, which does not have a mediator boson and therefore has no corresponding force, weak isospin does have mediator bosons, these are the W bosons. Similarly, the B boson acts on a quantity called *weak hypercharge*, denoted Y, which is -1 for left-handed leptons and $+\frac{1}{3}$ for left-handed quarks (antiparticles have the opposite weak hypercharge compared to the corresponding particles). Right-handed fermions have weak hypercharge equal to twice their electric charge. The weak hypercharge can be described by the group U(1), which is just the group of complex numbers with absolute value 1, meaning that the weak hypercharge is a scalar. None of the vector bosons have weak hypercharge. Since the photon is a superposition state of the B and W^0 bosons, it acts on a linear combination of weak hypercharge and weak isospin. This linear combination is called the *electric charge*, denoted Q, and is defined as

$$Q = w_z + \frac{1}{2}Y. \tag{2.16}$$

It is possible to define a "Z charge" for the Z boson in a similar way, however this is rarely useful since the Z boson is very massive, which means that it is hard to produce making its force very weak.

One other noticeable difference between spin and weak isospin is that while particles of the same type but different spin have the same masses, particles with different weak isospin have different masses. This is due to the Higgs boson, which, despite being a weak isospin singlet, has non-zero

weak isospin. The Higgs boson has $w_z = -\frac{1}{2}$, but there is no corresponding scalar boson with $w_z = +\frac{1}{2}$, meaning that the weak isospin SU(2) symmetry is broken. This means that the Higgs boson interacts differently with particles with different weak isospin, giving them different masses. The Higgs boson also has a weak hypercharge equal to +1, which also breaks the weak hypercharge U(1) symmetry, since it has no antiparticle with weak hypercharge −1 (the Higgs boson is its own antiparticle). However, since the Higgs boson has zero electric charge, this creates a new symmetry under electromagnetic U(1). By Noether's theorem, this means that electric charge must be conserved, while weak isospin and weak hypercharge do not need to be conserved.

Another aspect of symmetry breaking is that while spin can be measured along any axis, weak isospin must be measured along one specific axis. If we try to measure the weak isospin along a different axis, we would get a superposition state of particles with different masses, which is not a mass eigenstate and therefore not physical. This comes from the fact that the Higgs boson has a well-defined w_z, but there is no corresponding particle with a well-defined w_x or w_y. So while we can choose the spin axis ourselves, the weak isospin axis is fixed by the Higgs boson. This also means that multiplying a weak isospin vector with an arbitrary SU(2) matrix does not necessarily result in a physical state, so the Standard Model is not symmetric under weak isospin SU(2).

2.1.2 The SU(3) group: a mathematical model for QCD

Quantum chromodynamics, or *QCD*, is the name of the theory describing the strong force. The name comes from the fact that quarks are said to carry *color charge*, as we will see later in this section.

Just like the electroweak force can be described using the SU(2) group, QCD can be described using the SU(3) group. However, unlike electroweak SU(2), the SU(3) symmetry is not broken, so while each quark comes in three different so-called color charges, they are commonly considered the same type of particle since they have the same mass.

For SU(3), the generating matrices are the *Gell-Mann matrices* $\lambda_1, \ldots, \lambda_8$:

$$\lambda_1 = \begin{pmatrix} 0 & 1 & 0 \\ 1 & 0 & 0 \\ 0 & 0 & 0 \end{pmatrix} \quad \lambda_2 = \begin{pmatrix} 0 & -i & 0 \\ i & 0 & 0 \\ 0 & 0 & 0 \end{pmatrix} \quad \lambda_3 = \begin{pmatrix} 1 & 0 & 0 \\ 0 & -1 & 0 \\ 0 & 0 & 0 \end{pmatrix} \quad \lambda_4 = \begin{pmatrix} 0 & 0 & 1 \\ 0 & 0 & 0 \\ 1 & 0 & 0 \end{pmatrix} \tag{2.17}$$

$$\lambda_5 = \begin{pmatrix} 0 & 0 & -i \\ 0 & 0 & 0 \\ i & 0 & 0 \end{pmatrix} \quad \lambda_6 = \begin{pmatrix} 0 & 0 & 0 \\ 0 & 0 & 1 \\ 0 & 1 & 0 \end{pmatrix} \quad \lambda_7 = \begin{pmatrix} 0 & 0 & 0 \\ 0 & 0 & -i \\ 0 & i & 0 \end{pmatrix} \quad \lambda_8 = \frac{1}{\sqrt{3}} \begin{pmatrix} 1 & 0 & 0 \\ 0 & 1 & 0 \\ 0 & 0 & -2 \end{pmatrix}.$$

Just like the Pauli matrices, the Gell-Mann matrices can be combined into ladder operators:

$$\hat{T}_+ = \frac{1}{2}(\lambda_1 + i\lambda_2) \qquad \hat{T}_- = \frac{1}{2}(\lambda_1 - i\lambda_2) \qquad \hat{T}_z = \frac{1}{2}\lambda_3 \tag{2.18}$$

$$\hat{U}_+ = \frac{1}{2}(\lambda_6 + i\lambda_7) \qquad \hat{U}_- = \frac{1}{2}(\lambda_6 - i\lambda_7) \qquad \hat{U}_z = \frac{\sqrt{3}}{2}\lambda_8 - \frac{1}{2}\lambda_3 \tag{2.19}$$

$$\hat{V}_+ = \frac{1}{2}(\lambda_4 + i\lambda_5) \qquad \hat{V}_- = \frac{1}{2}(\lambda_4 - i\lambda_5) \qquad \hat{V}_z = \frac{\sqrt{3}}{2}\lambda_8 + \frac{1}{2}\lambda_3. \tag{2.20}$$

Since $\hat{T}_z$, $\hat{U}_z$ and $\hat{V}_z$ commute, they have common eigenstates. We call these eigenstates $|t_z, u_z, v_z\rangle$ where t_z, u_z and v_z are the eigenvalues of $\hat{T}_z$, $\hat{U}_z$ and $\hat{V}_z$ respectively. This works similarly to spin, where $\hat{S}_z$ an be used to measure the spin s_z of a state along the z-axis, and $\hat{S}_\pm$ can be used to increase or decrease the spin of that state. Since SU(3) symmetry is not broken, using the z-axis is just a convention, any other axis could be chosen by ordering the Gell-Mann matrices differently.

One can then prove that the ladder operators act on this state in the following way:

$$\hat{T}_\pm |t_z, u_z, v_z\rangle \propto \left| t_z \pm 1, u_z \mp \frac{1}{2}, v_z \pm \frac{1}{2} \right\rangle, \tag{2.21}$$

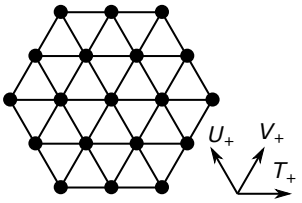

Figure 2.2: Graphical representation of the eigenstates of $\hat{T}_z$, $\hat{U}_z$ and $\hat{V}_z$. Acting with the ladder operators corresponds to moving the eigenstates in the direction of the corresponding arrow.

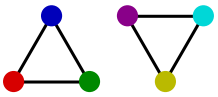

Figure 2.3: Graphical representation of the three quark states (left) and anti-quark states (right). Here anti-colors are represented by the complement of the corresponding color (anti-red = cyan, anti-green = magenta, anti-blue = yellow).

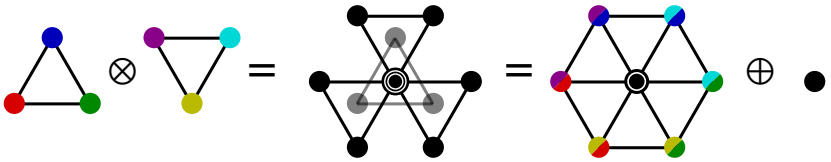

Figure 2.4: Graphical representation of quark-antiquark two-particle states.

and similarly for $\hat{U}_\pm$ and $\hat{V}_\pm$. This means that the eigenstates of $\hat{T}_z$, $\hat{U}_z$ and $\hat{V}_z$ can be represented in a hexagonal lattice as shown in Figure 2.2.

In the SU(2) case, for a given spin, there are only a finite number of s_z states a particle can have. For example, a fermion can only have two states, spin up and spin down. Similarly, in SU(3), the lattice mentioned above is finite. Just like in equation (2.8), if we act with a latter operator on a state in a way that would leave the lattice, the result is zero.

The smallest possible such lattice is the trivial lattice with only one point. This is called an *SU(3) singlet*. In QCD, this corresponds to particles that do not interact strongly and have no color charge at all, such as leptons or photons.

There are two ways of drawing the smallest possible non-trivial lattice: a right side up triangle and an up side down triangle, as shown in Figure 2.3. These are called *SU(3) triplets*, and one corresponds to quarks and the other to antiquarks. The three quark states are commonly referred to as red, green and blue, and the anti-quark states as anti-red, anti-green and anti-blue. This is called color charge.

The possible two-particle states can be obtained by taking the diagram of one particle, and replacing each point on that diagram with the diagram of the other particle, as shown in Figure 2.4 (mathematically, this corresponds to taking the tensor product). When we do so, we get nine states, six on the outside and three in the middle.

Of the three states in the middle, one of them corresponds to the SU(3) singlet state, and is truly colorless. The two others, while they do not have any t_z, u_z or v_z components, are still not truly colorless and can still interact strongly. This can be compared to a spin-1 state with $s_z = 0$. While the s_z component of the spin is zero, s is 1, so the particle still has a non-zero spin.

We can separate these nine states into the singlet state and the eight other states, which form an SU(3) octet. This is comparable to two spin-$\frac{1}{2}$ particles together forming a spin-0 singlet and a spin-1 triplet.

Hadrons are groups of quarks that form an SU(3) singlet. The SU(3) singlet obtained by combining a quark and an antiquark as above is called a meson. There are also baryons, which are SU(3) singlet states obtained by combining three quarks. This can be done following a process similar to the above, but with three particles instead of two: first combine two quarks (not a quark and an antiquark) using a similar process to the above, then add a third quark. This will give 27 states, which can be split into an octuplet (18 states), an octet and a singlet.

Similarly to the SU(2) case where the singlet state is $\frac{1}{\sqrt{2}}(|\uparrow\downarrow\rangle - |\downarrow\uparrow\rangle)$, one can prove that in the SU(3) case, the singlet states are given by

$$q\bar{q} = \frac{1}{\sqrt{3}}(|r\bar{r}\rangle + |g\bar{g}\rangle + |b\bar{b}\rangle) \tag{2.22}$$

$$qqq = \frac{1}{\sqrt{6}}(|rgb\rangle - |rbg\rangle + |brg\rangle - |bgr\rangle + |gbr\rangle - |grb\rangle), \tag{2.23}$$

for mesons and baryons respectively.

While quarks form an SU(3) triplet, gluons, the mediators of the strong force, form an SU(3) octet. This is the same octet as the one above, which is why gluons are said to carry a color and an anti-color. Since gluons carry color, they can interact with themselves, which will have important consequences as we will see in the next chapter.

2.1.3 Color confinement and jets

To understand what consequences the gluon carrying color has on how the strong force behaves, we will look at a semi-classical picture where we compare QCD to classical electromagnetism.

In electromagnetism, photons do not interact with other photons, which allow the field lines to be spread out in space, as shown in figure 2.5a. This means that when two electric charges are separated from each other, the electric field felt by one particle from the other decreases as the electric field becomes more spread out. Mathematically, one can prove that the electric field E generated by a single charge decreases as $\frac{1}{r^2}$, where r is the distance from that object. This is called the inverse square law. If all particles are assumed to have a charge equal to the elementary charge, this gives:

$$E = \hbar c \alpha_{\text{EM}} \frac{1}{r^2}, \tag{2.24}$$

where $\hbar$ is the reduced Planck constant, c is the speed of light, and α_{EM} is the electromagnetic coupling constant, also known as the fine structure constant. A more familiar version of Coulomb's law can be found by rewriting equation (2.24) using the fact that $\hbar c \alpha_{\text{EM}} = \frac{e^2}{4\pi\varepsilon_0}$.

Integrating equation (2.24) with respect to r gives the potential energy felt by one particle due to the other:

$$V_{\text{EM}}(r) = \int E dr = -\hbar c \alpha_{\text{EM}} \frac{1}{r}. \tag{2.25}$$

This means that when we let the distance between two electric charges go to infinity, the potential energy between them converges, so if we have enough energy we can separate two electric charges arbitrarily far away from each other. This also means that if two electric charges are far enough away from each other, the force that they exert on each other becomes negligible, and so does the amount of energy required to increase the distance between them even more.

Gluons, on the other hand, carry color, so gluons of different colors are attracted to each other. This means that unlike electromagnetic field lines, strong field lines are not spread out in space,

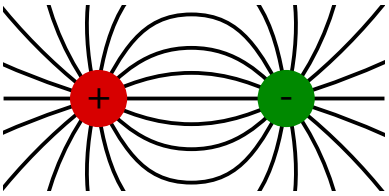

(a) Electromagnetic dipole field

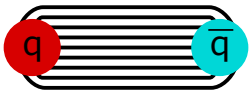

(b) Strong dipole field

Figure 2.5: Comparison of dipole fields for the electromagnetic force and the strong force.

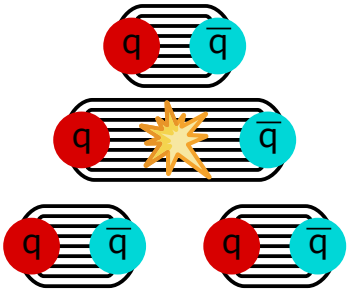

Figure 2.6: A quark and an antiquark are being pulled apart far enough for the potential energy between them to be sufficient to create a new quark-antiquark pair. (Explosion image from https://www.iconfinder.com/)

but instead form a tube of gluons between two quarks, as shown in figure 2.5b. The radius of the tube does not depend on the distance between the two quarks, so as the distance increases, the gluon field does not become more spread out and does not decrease, but is constant. This means that in addition to the inverse square law (which is always there), the gluon field also has a constant term κ (which can be measured to be of the order of magnitude of 1 GeV/fm):

$$G = \frac{4}{3}\hbar c \alpha_{\text{QCD}} \frac{1}{r^2} + \kappa, \tag{2.26}$$

where G denotes the strong force equivalent of the electric field, and α_{QCD} is the strong coupling constant. The $\frac{4}{3}$ factor comes from the fact that QCD can be described with SU(3) while electromagnetism can be described with U(1).

Again, we can take the integral of this with respect to r to get the potential energy:

$$V_{\text{QCD}}(r) = \int G dr = -\frac{4}{3}\hbar c \alpha_{\text{QCD}} \frac{1}{r} + \kappa r. \tag{2.27}$$

This means that at distances large enough for the $\frac{1}{r}$ term to be negligible, the potential energy between two quarks increases linearly as a function of the distance between those quarks. So if two quarks are pulled apart far enough, the potential energy between them will eventually become larger than the energy needed to create a new quark-antiquark pair. At that point, a pair will be created, which will form new hadrons, as shown in Figure 2.6.

This means that below an energy scale Λ_{QCD} called the *confinement scale* (which is of the order of magnitude of 100 MeV [6]), the only stable groups of quarks are those that do not interact strongly. Since the SU(3) singlet is the only configuration that does not have any net color and therefore does not interact strongly, all quarks in nature must be confined into this configuration, called a hadron. This is called *color confinement*.

The reason why this is only valid below the confinement scale is because at very high energies the coupling constant α_{QCD} diverges, causing the inverse square term in equation (2.26) to dominate.

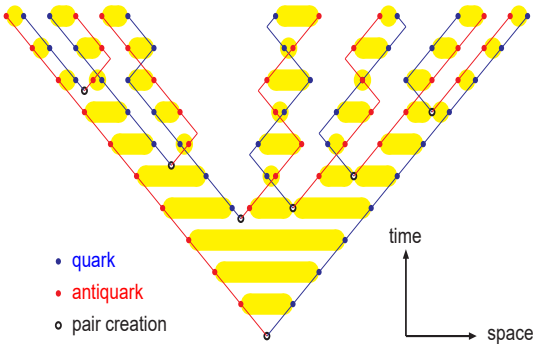

Figure 2.7: Illustration of a quark and an antiquark fragmenting into jets. Yellow lines represent strings of gluons. Source: [7]

The reason why the strong force described by SU(3) is different from the electroweak force described by SU(2) is because the gluons are massless while the W bosons are massive. Since the W bosons are massive, they will decay before being able to form tubes like the ones shown in Figure 2.5b. While photons, which are massless, have an SU(2) component through the W^0 boson, this is not enough for them to be self-interacting since the $W^{\pm}$ bosons are massive.

At the LHC, the energy is sufficient for this process to happen many times, as shown in Figure 2.7. The reason it happens many times is because after it has happened once, the quarks in the first hadron will still have relative momentum with respect to each other. It can also happen that multiple quark-antiquark pairs are created at causally disconnected points, which is the case for the lowest pair creation points in Figure 2.7.

This means that when two quarks go away from each other at very high energies at the LHC (for example because they are decay products of a significantly heavier particle), many mesons are produced this way (most of these mesons consist of new quarks produced in the process illustrated in Figure 2.6, not the original quarks). It can also happen, though more rarely, that several quark-antiquark pairs are produced at once, which can produce baryons. Some of these hadrons are unstable and can decay into lighter hadrons, photons or leptons. This means that it is common at the LHC to observe a collimated stream of particles, which is called a *jet*. The fact that they often reach the detector in a small space is due to conservation of momentum, since the new quark-antiquark pairs will often move in the same direction as the other quarks.

High energy mesons are more likely to split further into new quark-antiquark pairs than low-energy mesons. This is because it is more likely for the gluon tubes to gain enough energy to create new quark-antiquark pairs. This is illustrated in Figure 2.7, where we see that more quark-antiquark pairs are created on the sides of the figure, which represents the particles moving faster.

2.1.4 Types of hadrons

As we saw previously, hadrons can be split into two types: baryons, which contain three quarks, and mesons, which contain a quark and an antiquark. As we can see in Figure 2.1, there are six types of quarks, five of which can form hadrons. The top quark, being more massive than the W boson, can decay directly into an on-shell W boson and a bottom quark, making it too short-lived to interact with other quarks and therefore form hadrons.

Since there are five types of quarks that can form hadrons, there are many different ways they can be combined, giving rise to many different types of hadrons, each with their own mass. While it is not very useful to know the names of all types of hadrons that can possibly exist, it can be useful to know the most common ones. In nature, the most common hadrons are the proton, consisting of two up quarks and a down quark, and the neutron, consisting of two down quarks and an up

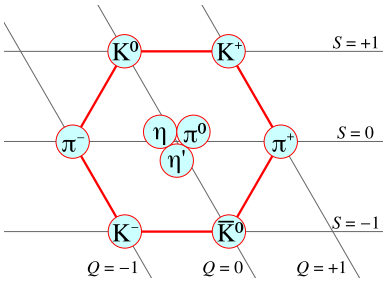

Figure 2.8: Lightest pseudo-scalar mesons grouped by electric charge Q and strangeness S. Source: Wikipedia

quark. Both the proton and the neutron are therefore baryons. In this thesis, the mesons are especially important, so in this chapter we will go through the most common mesons, which are the ones containing up, down or strange quarks.

As we saw in section 2.1.1, a two-fermion state can have either spin 0 or spin 1. This means that there are two types of mesons: *pseudo-scalar mesons*, which have spin 0, and *vector mesons*, which have spin 1. Vector mesons are more massive than pseudo-scalar mesons, and will often decay very quickly into pseudo-scalar mesons.

The lightest pseudo-scalar mesons are called *pions*, and are made of first generation quarks. The π^+ has quark content $u\bar{d}$, and its antiparticle, the π^-, has quark content $d\bar{u}$. The π^0 is a superposition state of $u\bar{u}$ and $d\bar{d}$:

$$\pi^0 = \frac{1}{\sqrt{2}}(u\bar{u} - d\bar{d}). \tag{2.28}$$

Pure $u\bar{u}$ and $d\bar{d}$ states are not mass eigenstates. The other neutral pseudo-scalar meson with $u\bar{u}$ and $d\bar{d}$ states mixes with the $s\bar{s}$ state to form the two eta mesons:

$$\eta = \frac{1}{\sqrt{6}}(u\bar{u} + d\bar{d} - 2s\bar{s}) \qquad \eta' = \frac{1}{\sqrt{3}}(u\bar{u} + d\bar{d} + s\bar{s}). \tag{2.29}$$

Finally, it is possible to combine a strange quark with a first generation quark to form *kaons*. The K^+ has a quark content $u\bar{s}$ and its antiparticle, the K^-, has a quark content $s\bar{u}$. Neutral kaons can be formed by combining a down quark with a strange quark: $K^0 = d\bar{s}$ and $\bar{K}^0 = s\bar{d}$. However, the K^0 and $\bar{K}^0$ are not CP eigenstates. Since CP must at first approximation be conserved, this means that they do not have a definite decay mode, and therefore not a definite lifetime. Instead, the states that have a definite lifetime are

$$K_L^0 \approx \frac{1}{\sqrt{2}}(d\bar{s} + s\bar{d}) \qquad K_S^0 \approx \frac{1}{\sqrt{2}}(d\bar{s} - s\bar{d}), \tag{2.30}$$

where L is as in "long" since this is the one with longer lifetime, and S is as in "short" since this is the one with the shorter lifetime. The K_S^0 has $CP = +1$ and the K_L^0 has $CP = -1$. Since both decay into pions and one pion has $CP = -1$ (CP is multiplicative), this means that the K_S^0 decays into two pions and the K_L^0 primarily decays into three pions, which explains why the K_L^0 has a longer lifetime. This is however just an approximation: the K_L^0 can decay into two pions as well causing CP violation, this is however suppressed, so it still has a longer lifetime than the K_S^0.

These pseudo-scalar mesons can be grouped together using strangeness and electric charge as shown in Figure 2.8. The similarity with Figure 2.4 is not a coincidence: up, down and strange quarks can be described by an SU(3) group (although not a fundamental one like QCD, spin or weak isospin). In this group, the η' meson would be the singlet and the other eight pseudo-scalar mesons would form an octet. It is important to note that this is not the same as the QCD SU(3) group (even though they have the same structure): all mesons (and in general all hadrons) are singlets under QCD.

In addition to pseudo-scalar mesons that have spin 0, there are also vector mesons with spin 1. The lightest vector mesons are the *rho mesons* ρ^+, ρ^- and ρ^0. These have exactly the same quark content as the corresponding pions, the only difference being their spin.

Unlike for the pseudo-scalar mesons, the spin-1 $s\bar{s}$ state does not mix the the first generation quarks, but instead has its own mass eigenstate, called the *phi meson*. This means that there is an additional vector meson made only of first generation quarks, the *omega meson*:

$$\omega = \frac{1}{\sqrt{2}}(u\bar{u} + d\bar{d}). \tag{2.31}$$

Here we see that the SU(3) symmetry of the *uds* quarks is broken by the higher mass of the strange quark, and leaves us instead with an SU(2) symmetry between up and down quarks, where the rho mesons form a triplet and the omega meson forms a singlet. This SU(2) symmetry is sometimes referred to as *strong isospin*, but unlike weak isospin, it is not fundamental.

Note that in strong isospin SU(2), the singlet state is $\omega = \frac{1}{\sqrt{2}}(u\bar{u} + d\bar{d})$ (with a plus sign), whereas for spin SU(2), the singlet state is $\frac{1}{\sqrt{2}}(|\uparrow\downarrow\rangle - |\downarrow\uparrow\rangle)$ (with a minus sign). This is because mesons are made of a quark and an antiquark, and strong isospin changes sign under charge conjugation, which leads to an extra minus sign in one of the terms in equation (2.13). This is the same reason why equation (2.22) is symmetric while equation (2.23) is antisymmetric.

Finally, the spin-1 equivalent of the kaons are the K^* *mesons*: K^{*+}, K^{*-}, K^{*0} and $\bar{K}^{*0}$. Unlike the neutral kaons, the neutral K^*s do not mix, and the K^{*0} and $\bar{K}^{*0}$ both have definite lifetimes. The reason for this is that even though they are not CP eigenstates, they primarily decay into a pseudo-scalar kaon and a pion [8], and since the kaon is not a CP eigenstate either, this decay mode is possible regardless of CP.

2.2 Dark QCD

The Standard Model is very good at explaining most things we observe, but not all. One thing that cannot be explained by the Standard Model is dark matter. We have good reasons to suspect that dark matter is made of one or more new particles that we have not discovered yet. If there is at least one particle that we have not discovered yet, there might be many of them. This would mean that there could be an entire *dark sector* that we have not discovered yet, which contains stable particles that could be dark matter candidates, but also unstable particles.

One way this is possible is if the particles in the dark sector interact with each other through *dark QCD*, which would be a new force similar to Standard Model QCD that only interacts with dark particles [5]. In this hypothesis, there would be dark quarks (denoted q_{D}) that are confined into dark hadrons by dark QCD mediated by dark gluons (denoted g_{D}).

Just like Standard Model hadrons, dark hadrons can be split into two categories: dark mesons, which are made of a dark quark and a dark antiquark, and dark baryons, which are made of n_c dark quarks (where $n_c \geq 2$ is the integer such that dark QCD is described by SU(n_c)). Since at least some dark baryons would be stable, they would be the main dark matter candidate. However, since dark mesons would be more prevalent at the LHC, they are of more interest in this thesis, even though they are often unstable meaning they are not good dark matter candidates. This can be compared with Standard Model QCD, where baryons make up matter while mesons are more prevalent at the LHC. In the models we will look at, for simplicity, we will neglect dark baryons entirely and only consider dark mesons [5].

2.2.1 Parameters of dark QCD

While Standard Model QCD can be described by the SU(3) group, dark QCD can more generally be described by the SU(n_c) group, where $n_c \geq 2$ is the number of colors [5]. If $n_c = 3$, dark

Table 2.1: A summary of the dark mesons that will be studied in this thesis.

Dark meson	Spin	Dark charge
$\pi_{\mathrm{D}}^{\text{“0”}}$	0	0
$\pi_{\mathrm{D}}^{\text{“}\pm\text{”}}$	0	± 1
$\rho_{\mathrm{D}}^{\text{“0”}}$	1	0
$\rho_{\mathrm{D}}^{\text{“}\pm\text{”}}$	1	± 1

QCD would be able to be described in the same way as Standard Model QCD was described in section 2.1.2. If $n_c = 2$, dark color would be similar to weak isospin, however, since the dark gluon is massless unlike Standard Model W bosons, there would be confinement. If $n_c \geq 4$, dark QCD would be more complicated than Standard Model QCD, but the general ideas would be the same. In this thesis, however, we will only consider dark QCD models described by SU(2) or SU(3).

In the Standard Model, there are six types of quarks, with three generations (I, II and III in figure 2.1), where each generation is split into two quark types by the symmetry-broken electroweak SU(2), and where electromagnetism can be described by U(1). In this thesis, we will assume that the dark sector follows a similar structure, with n_g generations of dark quarks (the value of n_g depends on the model), each split into two dark quark types by a U(1) group [9]. Since each generation is split into two dark quark types, the number of dark flavors n_f is equal to $2n_g$. This is similar to the Standard Model, where there are three generations (I, II and III in Figure 2.1) but six flavors (u, d, s, c, b, t).

The dark U(1) symmetry cannot be the electromagnetic or weak U(1) from the Standard Model, since we know that dark matter does not have any electric charge. This means that dark quarks are singlets under electroweak U(1) and SU(2) and have zero weak hypercharge, weak isospin and electric charge, but have a “dark charge” of $\pm\frac{1}{2}$. For simplicity, we will assume that there are no dark leptons. In most models we will consider, dark U(1) symmetry will be broken meaning that dark charge does not have to be conserved, but in two models, dark charge will be conserved.

We will assume that the difference in mass between dark quarks with different dark charges is negligible. We will also neglect dark quarks that are heavier than the first generation. These two assumptions allow us to refer to the first generation quarks as a single particle, which we will simply call “dark quark” (denoted q_{D}). However, while the dark U(1) symmetry breaking is assumed to have a negligible effect on the masses of the dark quarks themselves, in two models, they do not have a negligible effect on the masses of the dark mesons. This means that in those models we will have dark mesons with different masses differing only by dark charge.

This means that we will look at a total of six dark mesons: the spin-0 dark pions, $\pi_{\mathrm{D}}^{\text{“}\pm\text{”}}$ and $\pi_{\mathrm{D}}^{\text{“0”}}$, and the spin-1 dark rho mesons, $\rho_{\mathrm{D}}^{\text{“}\pm\text{”}}$ and $\rho_{\mathrm{D}}^{\text{“0”}}$. The quotes around “ $\pm$ ” and “0” indicate that they do not relate to Standard Model electric charge but to dark charge. All particles in the dark sector have an electric charge of zero. We will neglect the dark sector equivalents of the eta and omega mesons.

It is possible that the mass of a dark hadron is different than the masses of its constituent quarks. It can be greater if the confined dark quarks gain a constituent mass through the uncertainty principle (similarly to how Standard Model quarks are more massive when they are confined inside hadrons), or smaller if the binding energy between the dark quarks is significant. Both phenomena always exist, but depending on which one is more important, the mass of the dark hadron can be greater or smaller than the mass of its constituents [10]. This is unlike the case of the Standard Model, where all hadrons have a mass greater than the mass of their constituents.

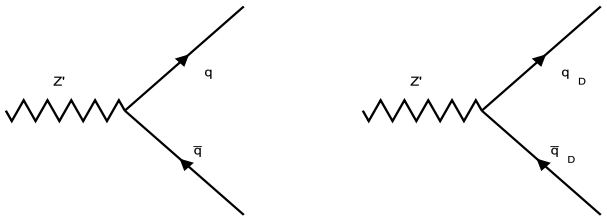

Figure 2.9: The possible vertices of the Z' boson. q denotes any Standard Model quark, and q_{D} denotes any dark quark.

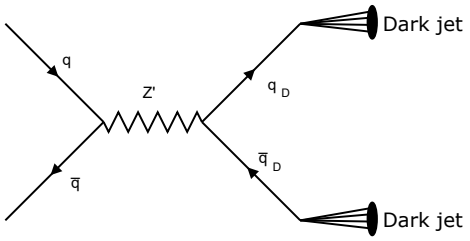

Figure 2.10: Feynman diagram showing how dark jets could be produced through the Z' boson at the LHC.

2.2.2 Dark matter portals

If we are going to have any chance of observing dark particles at the LHC, they have to somehow interact with Standard Model particles to be produced. Therefore, in all the models we will consider, we will assume that there is some type of new boson that can interact with both dark quarks and Standard Model particles. In the different models we will look at, there are three types of portal bosons: the Z' boson, the dark photon (denoted γ') and the X' boson.

The Z' boson has spin 1, is electrically neutral and has no dark color or Standard Model color. It has an interaction Lagrangian given by

$$\mathcal{L}_{\mathrm{int}} = \lambda \bar{q} \not{Z}' q + \lambda_{\mathrm{D}} \bar{q}_{\mathrm{D}} \not{Z}' q_{\mathrm{D}}, \tag{2.32}$$

where both terms have implicit sums over all flavors and colors. $\not{Z}' = \gamma^\mu Z'_\mu$ is the scalar product of the Z' field with the Dirac γ-matrices, q are the fields of the Standard Model quarks, and q_{D} are the fields of the dark quarks. λ is the coupling of the Z' boson with the Standard Model quarks, and λ_{D} is the coupling of the Z' boson with the dark quarks. This Lagrangian gives rise to the Feynman diagram vertices in Figure 2.9. A Feynman diagram is a diagram that illustrates how elementary particles interact with each other. Each particle has a finite set of Feynman diagram vertices, which can then be put together to illustrate a process. For example, the two vertices in Figure 2.9 can be put together to form the Feynman diagram in Figure 2.10.

The Z' boson can be considered to be the force mediator of dark charge [11]. Since the Z' boson can also interact with Standard Model quarks, this would mean that Standard Model quarks would also have a dark charge. However, since dark charge is described by U(1), all Standard Model quarks can have the same dark charge (just like they have the same weak hypercharge) meaning that there would not be multiple degenerate states of Standard Model quarks that we do not know of. Since the Z' boson has a large mass, the force that it mediates would be negligible. Therefore, Standard Model quarks having a dark charge would not cause any inconsistencies with the Standard Model as we know it.

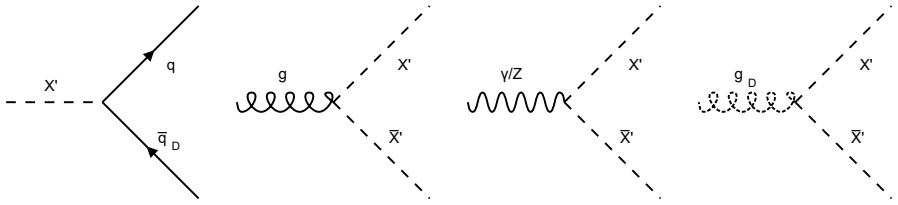

Figure 2.11: The possible vertices of the X' boson. q denotes any Standard Model quark, and q_{D} denotes any dark quark. g_{D} denotes the dark gluon.

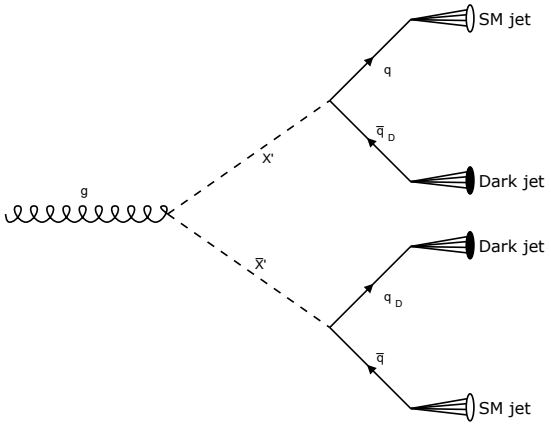

Figure 2.12: Feynman diagram showing how dark jets could be produced through the X' boson at the LHC.

At the LHC, considering resonant production, dark quarks could be produced by two Standard Model quarks interacting to form a Z' boson, and the Z' boson decaying into two dark quarks [12] (Figure 2.10). This means that in such models, we expect a dijet topology, where both jets are dark jets. In all models where the Z' boson is present, $\lambda_{\mathrm{D}} \gg \lambda$, which means that the Z' boson is significantly more likely to decay into dark quarks than to decay back into Standard Model quarks. All models we will use with a Z' boson have a branching ratio of the Z' boson into dark quarks of 99.9%, and a 0.1% branching ratio back into a Standard Model quark-antiquark pair.

In addition to the Z' boson, some models can also have a dark photon, denoted γ' [13]. The dark photon behaves very similarly to the Z' boson, but can also interact with charged leptons. The dark photon is assumed to have a significantly smaller mass than the Z' boson but also a significantly smaller coupling. The smaller coupling makes it more difficult to be produced at the LHC, but the smaller mass makes it more suitable as a decay mediator. This means that dark quarks at the LHC will always be produced through the Z' boson in models where it exists, but in the models that allow it, they will be able to decay through the dark photon into leptons.

Some models have an X' boson as a portal boson [14]. Unlike the Z' boson and the dark photon, the X' boson has spin 0 and carries both Standard Model color and dark anti-color, and has an electric charge of $-\frac{1}{3}$. It also has an antiparticle that carries a Standard Model anti-color and a dark color, and has an electric charge of $+\frac{1}{3}$. We assume that the X' boson is a singlet under electroweak SU(2), and that its electric charge originates entirely from its weak hypercharge. It has an interaction Lagrangian given by

$$\mathcal{L}_{\mathrm{int}} = \lambda d X' \bar{q}_{\mathrm{D}} + \lambda q_{\mathrm{D}} X'^{*} \bar{d}, \tag{2.33}$$

Table 2.2: Summary of all particles beyond the Standard Model used in this thesis. The PDG ID is a number unique for each particle type that is used by simulation and analysis software to keep track of which particle has which type.

Name	Symbol	Antiparticle	PDG ID	Models
Dark quark	q_{D}	$\bar{q}_{\mathrm{D}}$	4900101	All
Dark gluon	g_{D}	Self	4900021	All
Dark "neutral" pion	$\pi_{\mathrm{D}}^{\text{"0"}}$	Self	4900111	All
Dark "neutral" rho meson	$\rho_{\mathrm{D}}^{\text{"0"}}$	Self	4900113	All
Dark "charged" pion	$\pi_{\mathrm{D}}^{\text{"+"}}$	$\pi_{\mathrm{D}}^{\text{"-"}}$	4900211	All
Dark "charged" rho meson	$\rho_{\mathrm{D}}^{\text{"+"}}$	$\rho_{\mathrm{D}}^{\text{"-"}}$	4900213	All
Dark photon	γ'	Self	4900022	C-D, SVJL
Z' boson	Z'	Self	4900023	A-E, SVJ, SVJL
X' boson	X'	$\bar{X}'$	4900001	EJ1-EJ4

where both terms have implicit sums over all dark flavors. Since the X' boson comes in different colors, q_{D} is the dark quark field with the same dark color as that particular X' boson, and d is the Standard Model down quark field with the same color as that particular X' boson (we assume for simplicity that the X' boson can only couple to down quarks). Again, λ is a coupling constant. This Lagrangian gives rise to the first Feynman diagram vertex in Figure 2.11.

Since the X' boson carries Standard Model color, dark color and weak hypercharge, it can also couple with the Standard Model gluon, the dark gluon, the Standard Model photon and the Standard Model Z boson, as shown in the three remaining Feynman diagrams in figure 2.11 (it can however not couple with the W bosons since it has no weak isospin). Experimentally, the most interesting of these is the coupling with the Standard Model gluon, since it means that a X'-anti-X' pair can be produced from a gluon at the LHC (theoretically this is also possible with a photon or a Z boson, but the strong force is stronger). This means that in such models, dark particles can be produced at the LHC through the process shown in Figure 2.12. Since there are four particles in the final state, this will give rise to four jets. Of those, two are pure Standard Model jets (originating from the Standard Model quarks), and two are dark jets (originating from the dark quarks) [14]. This means that in these models we expect a four jet topology.

While the X' boson carrying Standard Model color and dark anti-color may at first sight look similar to the gluon carrying Standard Model color and anti-color, the two are different. As we saw before, the gluon is an octet under Standard Model SU(3), and since it has no dark color, it is a singlet under dark SU(3). The X' boson, on the other hand, is a triplet under Standard Model SU(3) and a triplet under dark SU(3). Since Standard Model SU(3) and dark SU(3) are two distinct groups (even though they are isomorphic), this means that there are $3 \cdot 3 = 9$ X' bosons, while there are only eight gluons. There are also 9 anti-X' bosons that differ from the X' bosons by their weak hypercharge, unlike the gluons that are their own antiparticles.

In most models the dark mesons are unstable, however, their lifetime can vary depending on different parameters of the model. They may decay very quickly into Standard Model particles, in which case their decay products can be observed at the LHC, or they can have a very long lifetime and be considered stable at detector scales, in which case we would only see missing energy. It is also possible that some types of dark mesons decay quickly and some are stable at detector scales, in which case we will only be able to see part of the dark jet. These are called semi-visible jets.

2.2.3 Dark QCD models

In this thesis, we will look at eleven different models, which we call Models A-E, Model SVJ (as in semi-visible jet), Model SVJL (as in semi-visible jet with leptons) and Models EJ1-EJ4 (as in emerging jet). These models are summarized in Tables 2.3 and 2.4, and the general properties of

Table 2.3: Parameters of Models A-E and SVJ.

Model	Model A	Model B	Model C	Model D
Reference	[10]	[10]	[10]	[10]
Number of colors n_c	3	3	3	3
Number of flavors n_f	2	6	2	6
Confinement scale Λ_{D}	15 GeV	2 GeV	15 GeV	2 GeV
Portal bosons	Z' (1500 GeV)	Z' (1500 GeV)	Z' (1500 GeV) γ' (4.0 GeV)	Z' (1500 GeV) γ' (0.7 GeV)
Mass of dark quark	20 GeV	2 GeV	20 GeV	2 GeV
Mass of $\pi_{\mathrm{D}}^{\text{“}\pm\text{”}}$	10 GeV	2 GeV	10 GeV	2 GeV
Mass of $\pi_{\mathrm{D}}^{\text{“}0\text{”}}$	10 GeV	2 GeV	10 GeV	2 GeV
Mass of $\rho_{\mathrm{D}}^{\text{“}\pm\text{”}}$	50 GeV	4.67 GeV	50 GeV	4.67 GeV
Mass of $\rho_{\mathrm{D}}^{\text{“}0\text{”}}$	50 GeV	4.67 GeV	50 GeV	4.67 GeV
Lifetime of $\pi_{\mathrm{D}}^{\text{“}\pm\text{”}}$	0	0	0	0
Lifetime of $\pi_{\mathrm{D}}^{\text{“}0\text{”}}$	0	0	0	0
Lifetime of $\rho_{\mathrm{D}}^{\text{“}\pm\text{”}}$	0	0	0	0
Lifetime of $\rho_{\mathrm{D}}^{\text{“}0\text{”}}$	0	0	0	0
Decay products of $\pi_{\mathrm{D}}^{\text{“}+\text{”}}$	$c\bar{c}$	$s\bar{s}$	$\gamma'\gamma'$	$\gamma'\gamma'$
Decay products of $\pi_{\mathrm{D}}^{\text{“}0\text{”}}$	$c\bar{c}$	$s\bar{s}$	$\gamma'\gamma'$	$\gamma'\gamma'$
Decay products of $\rho_{\mathrm{D}}^{\text{“}+\text{”}}$	$\pi_{\mathrm{D}}^{\text{“}0\text{”}}\pi_{\mathrm{D}}^{\text{“}0\text{”}}$	$\pi_{\mathrm{D}}^{\text{“}0\text{”}}\pi_{\mathrm{D}}^{\text{“}0\text{”}}$	$\pi_{\mathrm{D}}^{\text{“}0\text{”}}\pi_{\mathrm{D}}^{\text{“}0\text{”}}$	$\pi_{\mathrm{D}}^{\text{“}0\text{”}}\pi_{\mathrm{D}}^{\text{“}0\text{”}}$
Decay products of $\rho_{\mathrm{D}}^{\text{“}0\text{”}}$	$\pi_{\mathrm{D}}^{\text{“}0\text{”}}\pi_{\mathrm{D}}^{\text{“}0\text{”}}$	$\pi_{\mathrm{D}}^{\text{“}0\text{”}}\pi_{\mathrm{D}}^{\text{“}0\text{”}}$	$\pi_{\mathrm{D}}^{\text{“}0\text{”}}\pi_{\mathrm{D}}^{\text{“}0\text{”}}$	$\pi_{\mathrm{D}}^{\text{“}0\text{”}}\pi_{\mathrm{D}}^{\text{“}0\text{”}}$
Decay products of γ'	N/A	N/A	See Table 2.5	See Table 2.5

Model	Model E	Model SVJ	Model SVJL
Reference	[10]	[15]	[16]
Number of colors n_c	3	2	3
Number of flavors n_f	6	2	2
Confinement scale Λ_{D}	2 GeV	0.1 GeV	10 GeV
Portal bosons	Z' (1500 GeV)	Z' (1500 GeV)	Z' (2000 GeV) γ' (0.15 GeV)
Mass of dark quark	2 GeV	10 GeV	10 GeV
Mass of $\pi_{\mathrm{D}}^{\text{“}\pm\text{”}}$	2 GeV	9.99 GeV	4.99 GeV
Mass of $\pi_{\mathrm{D}}^{\text{“}0\text{”}}$	2 GeV	20 GeV	10.0 GeV
Mass of $\rho_{\mathrm{D}}^{\text{“}\pm\text{”}}$	4.67 GeV	9.99 GeV	25.8 GeV
Mass of $\rho_{\mathrm{D}}^{\text{“}0\text{”}}$	4.67 GeV	20 GeV	25.8 GeV
Lifetime of $\pi_{\mathrm{D}}^{\text{“}\pm\text{”}}$	Stable	Stable	Stable
Lifetime of $\pi_{\mathrm{D}}^{\text{“}0\text{”}}$	Stable	0	0
Lifetime of $\rho_{\mathrm{D}}^{\text{“}\pm\text{”}}$	0	Stable	Stable
Lifetime of $\rho_{\mathrm{D}}^{\text{“}0\text{”}}$	0	0	0
Decay products of $\pi_{\mathrm{D}}^{\text{“}+\text{”}}$	Stable	Stable	Stable
Decay products of $\pi_{\mathrm{D}}^{\text{“}0\text{”}}$	Stable	$s\bar{s}$ (80%), $\pi_{\mathrm{D}}^{\text{“}+\text{”}}\pi_{\mathrm{D}}^{\text{“}-\text{”}}$ (20%)	$s\bar{s}$ (30%), $\pi_{\mathrm{D}}^{\text{“}+\text{”}}\pi_{\mathrm{D}}^{\text{“}-\text{”}}$ (70%)
Decay products of $\rho_{\mathrm{D}}^{\text{“}+\text{”}}$	$\pi_{\mathrm{D}}^{\text{“}0\text{”}}\pi_{\mathrm{D}}^{\text{“}0\text{”}}$	Stable	Stable
Decay products of $\rho_{\mathrm{D}}^{\text{“}0\text{”}}$	$\pi_{\mathrm{D}}^{\text{“}0\text{”}}\pi_{\mathrm{D}}^{\text{“}0\text{”}}$	$q\bar{q}$ (80%), $\rho_{\mathrm{D}}^{\text{“}+\text{”}}\rho_{\mathrm{D}}^{\text{“}-\text{”}}$ (20%)	$\gamma'\gamma'$
Decay products of γ'	N/A	N/A	e^+e^-

For the decay products of $\rho_{\mathrm{D}}^{\text{“}0\text{”}}$ in Model SVJ, q denotes any Standard Model quark except the top quark, with the 80% branching ratio evenly distributed between each of the five quark types (so 16% each).

Table 2.4: Parameters of EJ1-EJ4.

Model	Model EJ1	Model EJ2
Reference	[14]	[14]
Number of colors n_c	3	3
Number of flavors n_f	2	2
Confinement scale Λ_{D}	10 GeV	10 GeV
Portal bosons	X' (1400 GeV)	X' (1400 GeV)
Mass of dark quark	10 GeV	10 GeV
Mass of $\pi_{\mathrm{D}}^{\text{“}\pm\text{”}}$	5 GeV	5 GeV
Mass of $\pi_{\mathrm{D}}^{\text{“}0\text{”}}$	5 GeV	5 GeV
Mass of $\rho_{\mathrm{D}}^{\text{“}\pm\text{”}}$	20 GeV	20 GeV
Mass of $\rho_{\mathrm{D}}^{\text{“}0\text{”}}$	20 GeV	20 GeV
Lifetime of $\pi_{\mathrm{D}}^{\text{“}\pm\text{”}}$	20 mm/c	150 mm/c
Lifetime of $\pi_{\mathrm{D}}^{\text{“}0\text{”}}$	20 mm/c	150 mm/c
Lifetime of $\rho_{\mathrm{D}}^{\text{“}\pm\text{”}}$	0	0
Lifetime of $\rho_{\mathrm{D}}^{\text{“}0\text{”}}$	0	0
Decay products of $\pi_{\mathrm{D}}^{\text{”}+\text{”}}$	$d\bar{d}$	$d\bar{d}$
Decay products of $\pi_{\mathrm{D}}^{\text{“}0\text{”}}$	$d\bar{d}$	$d\bar{d}$
Decay products of $\rho_{\mathrm{D}}^{\text{”}+\text{”}}$	$\pi_{\mathrm{D}}^{\text{”}+\text{”}}\pi_{\mathrm{D}}^{\text{”}+\text{”}}$ (99.9%), $d\bar{d}$ (0.01%)	$\pi_{\mathrm{D}}^{\text{”}+\text{”}}\pi_{\mathrm{D}}^{\text{”}+\text{”}}$ (99.9%), $d\bar{d}$ (0.01%)
Decay products of $\rho_{\mathrm{D}}^{\text{“}0\text{”}}$	$\pi_{\mathrm{D}}^{\text{“}0\text{”}}\pi_{\mathrm{D}}^{\text{“}0\text{”}}$ (99.9%), $d\bar{d}$ (0.01%)	$\pi_{\mathrm{D}}^{\text{“}0\text{”}}\pi_{\mathrm{D}}^{\text{“}0\text{”}}$ (99.9%), $d\bar{d}$ (0.01%)
Decay products of γ'	N/A	N/A

Model	Model EJ3	Model EJ4
Reference	[14]	[14]
Number of colors n_c	3	3
Number of flavors n_f	2	2
Confinement scale Λ_{D}	40 GeV	1.6 GeV
Portal bosons	X' (1400 GeV)	X' (1400 GeV)
Mass of dark quark	40 GeV	1.6 GeV
Mass of $\pi_{\mathrm{D}}^{\text{“}\pm\text{”}}$	20 GeV	0.8 GeV
Mass of $\pi_{\mathrm{D}}^{\text{“}0\text{”}}$	20 GeV	0.8 GeV
Mass of $\rho_{\mathrm{D}}^{\text{“}\pm\text{”}}$	80 GeV	3.2 GeV
Mass of $\rho_{\mathrm{D}}^{\text{“}0\text{”}}$	80 GeV	3.2 GeV
Lifetime of $\pi_{\mathrm{D}}^{\text{“}\pm\text{”}}$	75 mm/c	75 mm/c
Lifetime of $\pi_{\mathrm{D}}^{\text{“}0\text{”}}$	75 mm/c	75 mm/c
Lifetime of $\rho_{\mathrm{D}}^{\text{“}\pm\text{”}}$	0	0
Lifetime of $\rho_{\mathrm{D}}^{\text{“}0\text{”}}$	0	0
Decay products of $\pi_{\mathrm{D}}^{\text{”}+\text{”}}$	$d\bar{d}$	$d\bar{d}$
Decay products of $\pi_{\mathrm{D}}^{\text{“}0\text{”}}$	$d\bar{d}$	$d\bar{d}$
Decay products of $\rho_{\mathrm{D}}^{\text{”}+\text{”}}$	$\pi_{\mathrm{D}}^{\text{”}+\text{”}}\pi_{\mathrm{D}}^{\text{”}+\text{”}}$ (99.9%), $d\bar{d}$ (0.01%)	$\pi_{\mathrm{D}}^{\text{”}+\text{”}}\pi_{\mathrm{D}}^{\text{”}+\text{”}}$ (99.9%), $d\bar{d}$ (0.01%)
Decay products of $\rho_{\mathrm{D}}^{\text{“}0\text{”}}$	$\pi_{\mathrm{D}}^{\text{“}0\text{”}}\pi_{\mathrm{D}}^{\text{“}0\text{”}}$ (99.9%), $d\bar{d}$ (0.01%)	$\pi_{\mathrm{D}}^{\text{“}0\text{”}}\pi_{\mathrm{D}}^{\text{“}0\text{”}}$ (99.9%), $d\bar{d}$ (0.01%)
Decay products of γ'	N/A	N/A

Table 2.5: Branching ratios of the dark photon in models where it exists.

Decay mode	Model C	Model D	Model SVJL
$\gamma' \to e^+e^-$	17%	15%	100%
$\gamma' \to \mu^+\mu^-$	17%	15%	-
$\gamma' \to \tau^+\tau^-$	10%	-	-
$\gamma' \to \pi^+\pi^-$	-	70%	-
$\gamma' \to u\bar{u}$	22%	-	-
$\gamma' \to c\bar{c}$	22%	-	-
$\gamma' \to d\bar{d}$	6%	-	-
$\gamma' \to s\bar{s}$	6%	-	-

the different particles that appear in these models are summarized in Table 2.2.

Models A-D are from [10]. In Models A and B, all dark mesons decay promptly via the Z' boson into Standard Model quarks. In Models C and D, all dark mesons decay promptly via the dark photon into Standard Model particles (quarks or charged leptons).

Model E is a modified version of Model B where dark pions are set to be stable. In reality, while they are not necessarily completely stable, it is possible that they have a longer lifetime than it takes for them to reach the detector, so it would look like they are stable to the detector. No other parameters from Model B have been changed in Model E. While this may not be completely realistic (since the parameters are in theory not independent), Model E is still good for showing what would happen if dark mesons have a very long lifetime.

In Models SVJ [15] and SVJL [16], dark "charged" mesons are assumed to be stable due to conservation of dark charge. This is the only model we consider where dark charge is assumed to be conserved. Dark "neutral" mesons can decay either into dark "charged" mesons or into Standard Model quarks or, in the case of the $\rho_{\mathrm{D}}^{\text{“0”}}$ in Model SVJL, dark photons. This means that part of the jet will be visible to the detector but not the other part, resulting in semi-visible jets.

Models EJ1-EJ4 are from [14], however their names have been changed in this thesis to avoid confusion with the models from [10]. Models EJ1 and EJ2 correspond to Model A in [14] with different lifetimes of the dark pion, Model EJ3 is Model D from [14] and Model EJ4 is Model E from [14].

In the emerging jet (EJ) models, a pair of X' bosons can be produced from a Standard Model gluon, then decaying into a total of two Standard Model quarks and two dark quarks, as shown in Figure 2.12. The dark quarks will then hadronize to form dark mesons. The dark mesons then decay into Standard Model quark-antiquark pairs by the two dark quarks in the dark mesons exchanging an X' boson, which turns them into Standard Model quarks. The lifetimes of the dark pions in these models are close to the amount of time it takes them to reach the detector from the interaction point, which is why these models produce emerging jets.

3 LHC physics

The *Large Hadron Collider*, or *LHC*, is a particle accelerator located at the European Organization for Nuclear Research (CERN) in Switzerland. It accelerates hadrons (often protons) to energies of the order of 10 TeV and collides them with the purpose of carrying out experiments in particle physics. One of the major achievements so far that resulted from the analysis of the LHC data was the discovery of the Higgs boson in 2012. Many physicists hope that it will help discover additional new particles and theories in the future, one such theory being dark QCD.

This chapter contains two sections. First, an overview of proton-proton collision is given, highlighting the complexity of such interactions and defining the particle level, which is of main importance for this work. This is followed by a short description of the experimental setup.

3.1 Physics of proton-proton collisions

When two protons collide at the LHC, they can interact either elastically or inelastically. The elastic interactions are more common, but are uninteresting since they do not produce any other particles.

We are normally interested in the inelastic collisions. Since the relative kinetic energy of the protons is significantly greater than each of their binding energies, they can split into their constituent quarks and gluons. Since there are several quarks and gluons in a proton, one pp interaction can have several hard processes, i.e. processes that occur directly between partons before anything decays or hadronizes, due to different partons participating in different interactions. Often, one of these processes is of more interest than the others. For example, Figure 3.1 shows a typical proton–proton collision. In this figure, the main process is the $gg \to t\bar{t}$ process, in which one of the incoming gluons originates directly from one of the beam protons and another gluon was emitted by a quark from the other beam proton. However, there are two other secondary processes happening here, originating from other partons: one where two gluons interact to produce a third gluon and a heavy meson, and one where a quark and a gluon undergo elastic scattering. In addition, several gluons are emitted without participating in any hard process. All this is due to the fact that protons are composite particles, which means that they have different partons that can participate in multiple interactions.

Due to the factors mentioned above, a typical LHC pp collision of interest produces several hundred observable particles. Many of these particles can be seen as unrelated to the underlying hard process of interest. A result of this, which can be seen as a disadvantage, is that the event signatures will be less clean, making it more difficult to identify the processes we are interested in. However, colliding composite particles like protons also has an advantage: we can probe many energy scales with a fixed beam energy, since different amounts of energy can go into different processes.

3.1.1 Parton, particle and reconstruction level

When two particles collide at the LHC, they undergo many interactions before they reach the detector. These interactions can by divided into three stages: the *parton level* (also called generator level), the *particle level* (also called hadron level or truth level) and the *reconstruction level*. Only the reconstruction level can actually be observed in experiments, the two other levels are only available in simulations.

The parton level only includes the so-called hard processes. For example, in the processes studied in this thesis, this is the X' or Z' boson decaying into dark quarks or Standard Model quarks. The final state of the parton level will in this case only include the quarks that have not yet hadronized, decayed, formed jets, or interacted in any other way. There can be several ways to define it more

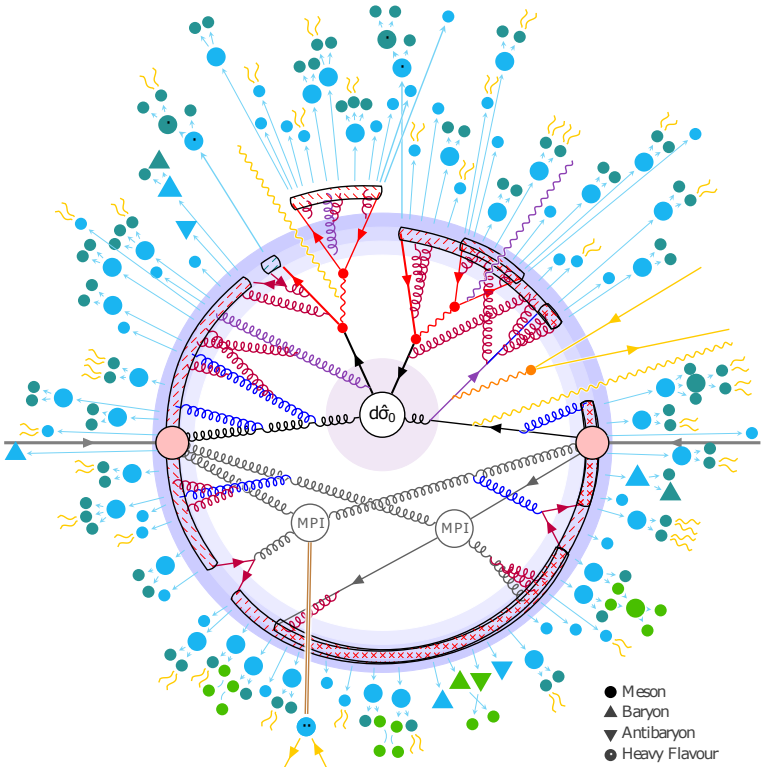

Figure 3.1: Illustration of a proton-proton collision event giving rise to the $gg \to t\bar{t}$ process. The process illustrated here is the following: the two beam protons (pink circles) collide and split into partons (black and gray). These partons emit gluons (blue) which do not participate in any interesting interaction. The main hard process occurs in the circle denoted "$d\hat{\sigma}_0$", where two gluons come together and produce a $t\bar{t}$ pair. Other hard processes occur in the background, denoted "MPI". The top quarks decay into bottom quarks and W bosons (red), and the W bosons decay further. Photons (yellow wavy lines), a Z boson (orange wavy line) and additional gluons (brown) are emitted. The Z boson decays into an electron-positron pair (yellow straight lines). When the partons reach the purple circle (which represents the boundary between parton level and particle level), they form hadrons (light blue circles and triangles). Some of these hadrons decay (dark green circles and triangles) or interact with each other (light green circles and triangles). Finally, some hadrons, mostly π^0's, decay into photons (yellow wavy lines). Source: [7]

precisely. In some cases the definition of the parton level can be extended to include initial and final state radiation (particles in dark blue and purple in Figure 3.1).

The particle level is defined by all particles produced by the pp collision in question that are stable at detector scales. A particle is considered stable at detector scales if it has a lifetime greater than the order of 10 mm/c, as we will see in the next section. Summing up the four momenta of all stable particles will always give $E = m = \sqrt{s}$ and $\vec{p} = \vec{0}$ (however a large fraction of this energy will be carried by beam remnants, which are particles that travel close to the beam pipe).

The reconstruction level is defined by the detector's measurements of the particles. Based on the measured detector signals, the particles are reconstructed as "physics objects". Each such reconstructed particle will be assigned a four-momentum, which, assuming calibration has been properly applied, should be close to the four-momentum at particle level. However, it will not be perfect for several reasons: The detector will have an intrinsic resolution, which will effectively "smear" the measured energy and momentum, and invisible particles such as neutrinos cannot be measured at all.

While the reconstruction level is the only level that is observable in the detector, it is possible to simulate the processes that happen in the collider, as we will do in this thesis. In simulations, it is possible to have access to all three levels.

3.1.2 Observable particles

A particle is said to be stable at detector scales if it lives long enough to have time to travel from the interaction point to the detector. As we saw in the previous section, these are the particles that are included in the particle level. At the ATLAS detector [17], the distance between the interaction point and the inner tracker is 33 mm [18], and the distance is similar in other detectors. Since most particles produced at the collider move close to the speed of light, this means that a particle can interact with the detector if its lifetime in the lab frame is greater than 33 mm/c.

In the Standard Model, the particles that are stable at detector scales are

- the photon, electron, proton and neutrino, which are completely stable
- the neutron and muon, which have a lifetime great enough that they will almost never spontaneously decay inside the detector
- the charged pions, charged kaons and the K_L^0, which have a lifetime slightly greater than needed to reach the calorimeters.

In addition, there are several Standard Model hadrons that have a lifetime of the order of a few mm/c, which is slightly shorter than needed to reach the detector. These are the K_S^0 and some baryons containing strange quarks: Λ^0 (uds), $\Sigma^\pm$ (uus or dds), Ξ^- (dss), Ξ^0 (uss) and Ω^- (sss). Since the lifetime of each individual particle is random, while the expectation of the lifetime of these particles is not enough to reach the detector, there can be individual particles of these types that live longer than expected and decay inside the detector. So it is not unusual to see these types of particles in the detector, especially considering the fact that relativistic time dilation can make them live longer in the lab frame.

Since neutral pions are unstable at detector scales, they will never be observed directly in the detector, instead their decay products will be observed. Since neutral pions most often decay into two photons, this means that it is very common to observe photons in jets, not just hadrons. Similarly, heavier hadrons consisting of charm or bottom quarks can have leptons as their decay products, so it is also possible to observe jets containing leptons. However, since these heavier hadrons are relatively uncommon, the lepton fraction of Standard Model jets is typically very low (although not zero).

In Model EJ1, the dark pions are in a situation similar to the Standard Model K_S^0 and strange baryons: their expected lifetime of 20 mm/c is shorter than the 33 mm/c to reach the inner tracker, but some individual particles can live long enough to reach the inner tracker. This means that in Model EJ1, we would expect to see jets that are partly invisible at the beginning of the inner tracker, but become completely visible in the outer layers of the detector. In Models EJ2-EJ4, the dark pions have a lifetime of $75 - 150$ mm/c, which means that most dark pions in these models would decay inside the inner tracker. This is why these models are called emerging jet models, since the jets emerge inside the detector.

3.1.3 Coordinate system

In many searches at the LHC, high energy particles are especially important since particles beyond the Standard Model are expected to have a very high mass. For example, when searching for dark QCD, the X' and Z' bosons are expected to be very massive, which means that particles originating from them would be very energetic.

The most obvious way of determining which particles are the most energetic would be to simply measure their energy or three-momentum. However, the protons themselves collide at very high energy, so it is possible to have particles with very high momentum in the beam direction which have not interacted in any meaningful way, but simply carry momentum left over from the beam protons. For this reason, we introduce *transverse momentum*, denoted p_{T}, which is defined as the component of the three-momentum perpendicular to the beam axis:

$$p_{\mathrm{T}} = \sqrt{p_x^2 + p_y^2}, \tag{3.1}$$

where p_x and p_y are the components of the three-momentum along the x- and y-axes in an orthonormal coordinate system where the beam axis is along the z-axis. That way, all particles must have gotten their p_{T} from the collision, since each of the beam protons have zero p_{T}.

To measure where the particle hits the detector, we use two coordinates: the *azimuth* ϕ and the *rapidity* y (not to be confused with the y-coordinate). As we will see in the next chapter, the detector is shaped as a cylinder. ϕ is simply defined as the angle around this cylinder, where $\phi = 0$ points in the positive direction of the y-axis. The rapidity is defined as

$$y = \operatorname{arctanh}\left(\frac{p_z c}{E}\right), \tag{3.2}$$

where p_z is the momentum of the particle along the beam axis and E is the energy of the particle. Assuming the particle was produced at the interaction point, its momentum will point from the interaction point to the point where it hits the detector. This means that the direction of its momentum $\frac{p_z}{p}$ can be used as a spatial coordinate, as well as the hyperbolic arctangent of this: $\eta = \operatorname{arctanh}(\frac{p_z}{p})$. η is commonly referred to as *pseudo-rapidity*. For very energetic particles, which includes most particles at the LHC that are stable at detector scales, $\frac{E}{c} \approx p$, which means that $y \approx \eta$. This means that the rapidity y can to a good approximation be used as a spatial coordinate. A rapidity of 0 means that the particle has momentum perpendicular to the beam line, so it hit the detector at the same z coordinate as the interaction point, and a rapidity of $\pm\infty$ means that the particle is moving along the beam line.

The rapidity y used in experimental particle physics should not be confused with the rapidity $w = \operatorname{arctanh}\left(\frac{v}{c}\right)$ used in special relativity. While these are different quantities, they have a similar definition: using that $E = \gamma mc^2$ and $p = \gamma mv$, the rapidity from special relativity can be written as $w = \operatorname{arctanh}\left(\frac{pc}{E}\right)$, which differs from equation (3.2) only by having the norm of the three-momentum p instead of the momentum along the beam axis p_z. This means that the rapidity we use in experimental particle physics can be seen as the z-component of the rapidity from special relativity.

The interest in using rapidity instead of the z-coordinate is that while the z-coordinate is measured in length units (usually centimeters or meters), the rapidity is dimensionless. Since the azimuth can be measured in radians, which can also be seen as a dimensionless quantity, this allows us to measure both coordinates of points in the detector in dimensionless quantities. This allows us to discuss these coordinates without having to worry about the size of the detector or which units we are using. Another advantage of the rapidity is that differences in rapidity are Lorentz invariant.

It is also possible to define a distance ΔR in y, ϕ-space between to objects i and j:

$$\Delta R_{i,j} = \sqrt{(y_i - y_j)^2 + (\Delta\phi_{i,j})^2}, \tag{3.3}$$

where $\Delta\phi_{i,j}$ is the difference in ϕ while taking into account the wrap-around effect.

It is common to plot events in event display plots with the rapidity on the x-axis and the azimuth on the y-axis. Examples of such plots are shown in the next chapter, for example in Figures 4.1 and 4.2. These plots can be seen as "unrolling" the detector as shown in Figure 3.2. When reading such plots, it is important to keep in mind that points at the top of the plot and the bottom of the plot are close to each other, which explains why one of the jets in Figure 4.2b is cut in half, with one half at the top and the other half at the bottom.

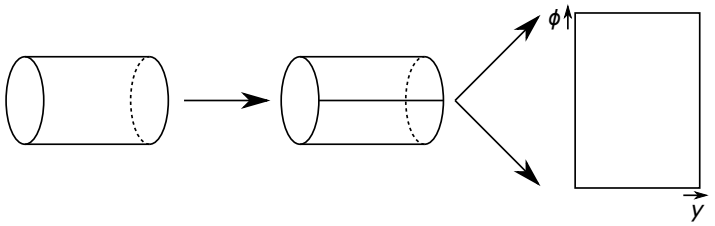

Figure 3.2: Event display plots can be seen as "unrolling" the cylinder-shaped detector.

3.1.4 Jet algorithms

As we saw in the theory section, a jet is a group of particles that can originate from the hadronization of a single parton. However, in general, it is not possible to be sure which final state particles originated from which parton. This means that an algorithm is needed to group particles together into jets.

Most such algorithms use a parameter called the *jet radius*, denoted R. This is a dimensionless quantity that corresponds to the size in y, ϕ space that jets are expected to have. R can be chosen to fit specific processes, and is typically chosen to be between 0.4 and 1. Larger values of the jet radius (often 1.0) are usually used for dijet-like events, whereas smaller values of the jet radius (often 0.4) are usually used in events with more complicated final states [7]. As we will see in the next chapter, this will also be the case in this thesis, where we will choose different values of the jet radius for different models.

The most common algorithms use a process called *sequential recombination*. This is implemented by defining a "distance" $d(i, j)$ between two constituents i and j and a "distance" $d(i, B)$ between a constituent i and the beam:

$$d(i,j) = \min({p_{\mathrm{T}}}_i^{2p}, {p_{\mathrm{T}}}_j^{2p}) \frac{\Delta R_{i,j}}{R} \tag{3.4}$$

$$d(i,B) = {p_{\mathrm{T}}}_i^{2p}, \tag{3.5}$$

where the exponent p is a parameter that depends on the algorithm, $\Delta R_{i,j}$ is the distance between the constituents defined in equation (3.3), and R is the jet radius.

In the algorithm, we start by defining the constituents to be the particles, loop over all constituents, and find the two constituents i and j that minimize $d(i, j)$, as well as the constituent k that minimizes $d(k, B)$. If $d(k, B) < d(i, j)$, we define k to be a jet. Otherwise, we repeat the process, but where we combine the two constituents i and j into a single constituent by summing their p_{T} and taking the weighted average of their y and ϕ.

This means that jets have four basic properties: the number of constituents n, the rapidity y which is the weighted average of the rapidity of its constituents, the azimuth ϕ which is the weighed average of the azimuth of its constituents, and the transverse momentum p_{T}, which is the sum of the transverse momentum of its constituents.

One major advantage with sequential recombination is that it is both infrared safe, which means that the output will not change significantly if a very low-energy particle is added to the input, and collinear safe, which means that the output will not change if a particle is split into two particles with the same y, ϕ and total p_{T}.

The two most common sequential recombination algorithms are the k_t *algorithm* and the *anti-*k_t *algorithm*. The k_t algorithm uses $p = 1$ and the anti-k_t algorithm uses $p = -1$. If we look at equation (3.4), if p is positive, particles with low p_{T} have a smaller $d(i, j)$ than particles with a high p_{T} and the same ΔR, and the opposite is true if p is negative. Since particles with smaller

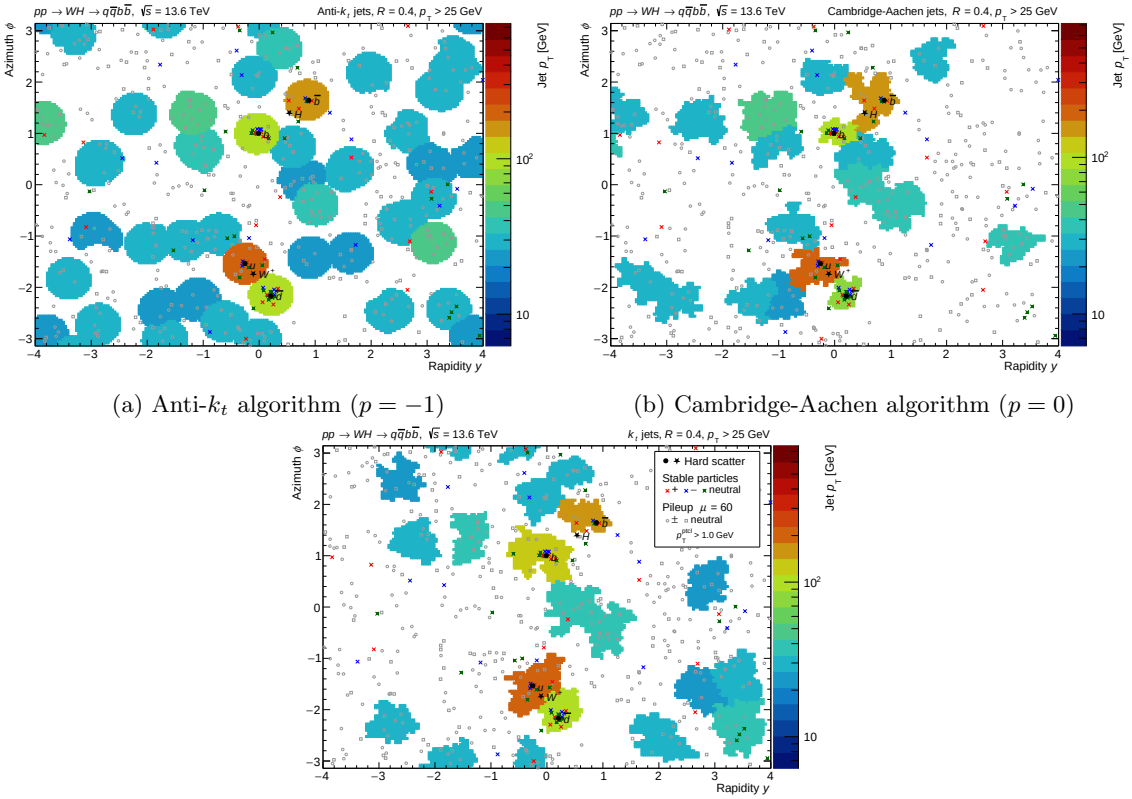

(a) Anti-k_t algorithm ($p = -1$)

(b) Cambridge-Aachen algorithm ($p = 0$)

(c) k_t algorithm ($p = 1$)

Figure 3.3: Event displays of the same event with jets built using different algorithms. The process displayed here has nothing to do with the processes studied in this thesis, it is only meant to illustrate the differences between the jet algorithms. The black markers indicate parton level particles. These plots were produced using Pythia's main95.cc example code [19].

$d(i,j)$ are processed first, this means that the k_t algorithm prioritizes low-p_T particles whereas the anti-k_t algorithm prioritizes high-p_T particles. This results in anti-k_t jets being nearly circular in y,ϕ-space, whereas k_t jets are more irregular, as we can see in Figure 3.3. It also shows the Cambridge-Aachen algorithm, which uses $p = 0$, which means that particles are not prioritized based on p_T at all. In all cases, the four highest p_T jets successfully capture the desired final state partons produced in the process (black circles). The assigned jet four momentum are also similar to those of the partons.

The anti-k_t algorithm is the one that is the most commonly used at ATLAS. There are two reasons for this: the regular jet shapes facilitate experimental analysis, and the anti-k_t algorithm is better than the others at building reconstruction level jets that match the particle level [7].

3.2 Experimental setup of the LHC

3.2.1 The LHC accelerator

The LHC consists of a 27 kilometer long ring [20]. It contains two beam pipes where the hadrons are accelerated, one for each direction. The hadrons are kept inside the beam pipes by using magnetic fields that have a strength that is exactly right to keep them inside the beam pipe.

The reason why the LHC is large is to limit the energy losses due to synchrotron radiation, which

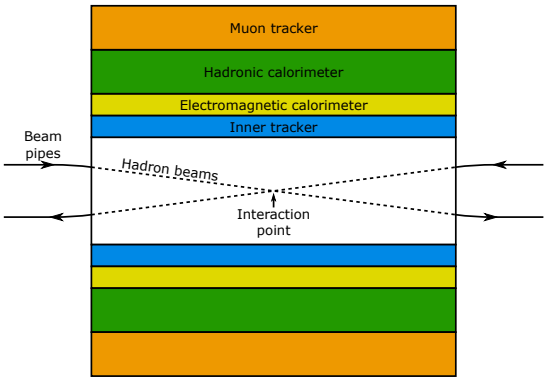

Figure 3.4: Simplified overview of the central, barrel of a multi-purpose particle detector. The trackers and calorimeters are wrapped around the beam line in a cylinder. This figure is not to scale, and the crossing angle has been exaggerated.

allows to accelerate the particles to higher energies, and therefore be able to produce more massive particles. The energy loss to synchrotron radiation per turn is equal to

$$-\Delta E = \frac{Q^2 E^4}{3\varepsilon_0 R m^4}, \tag{3.6}$$

where R is the radius of the accelerator, E is the energy of the particle being accelerated, m is its mass and Q is its electric charge.

We see here that a larger R leads to a smaller energy loss, which is why it is necessary to build a large accelerator. We also see that the more massive the particle is, the less energy will be lost. Other than the advantages of colliding composite particles to get wider ranges of energies as discussed in the previous chapter, this is another advantage of accelerating protons rather than electrons: since protons are more massive, they will lose less energy so they can be accelerated to higher energies than electrons.

3.2.2 Principle of a multi-purpose particle detector

The LHC has four different detectors: ATLAS, CMS, ALICE and LHCb [20]. ATLAS and CMS are general-purpose detectors, ALICE is specialized in studying QCD through quark-gluon plasma produced by colliding heavy ions, and LHCb is specialized in studying bottom and charm quarks.

Outside of the detectors the beam pipes are separated so that collisions cannot occur just anywhere, but inside each detector, the beams are focused so that the protons collide at an interaction point at the center of the detector. The detectors are shaped as a cylinder around this interaction point. Most detectors consist of four layers: the inner tracker, the electromagnetic calorimeter, the hadronic calorimeter and the muon tracker. A simplified drawing of how the main parts of the detector are set up is shown in Figure 3.4.

Each layer of the detector is built to identify different types of particles. The inner tracker is designed to tell the charge and three-momentum of a particle. It is made of a semiconductor material, so that charged particles passing through it create electron-hole pairs along their path, allowing us to measure their trajectory. Neutral particles on the other hand pass through without leaving any such track. There is a magnetic field in the tracker that causes oppositely charged particles to bend in opposite directions, allowing to tell if a particle is positively or negatively

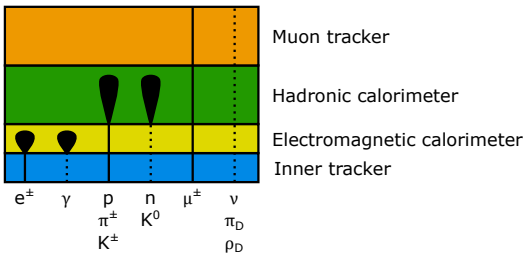

Figure 3.5: Most common interaction of different particles with the ATLAS detector. Dotted lines indicate particles passing through without interacting. π_D and ρ_D refer to the dark mesons in Models E, SVJ and SVJL discussed in section 2.2.3.

charged. The magnetic field also causes the trajectories of charged particles with lower momentum to bend faster, allowing to measure the momentum of the charged particles.

The electromagnetic calorimeter is designed to absorb and measure the energy of photons and electrons. This is done by the electrons interacting with the absorber plates and emit photons through bremsstrahlung, and the photons interacting with the material and produce electron-positron pairs. The particles that are emitted this way interact in the same way themselves, and the process repeats until most of the energy is deposited. This is called a *shower*.

Hadrons interact differently with the detector. Charged hadrons leave tracks in the inner tracker and can undergo bremsstrahlung, however less frequently than electrons due to their larger mass. The dominant interactions between incident hadrons with the calorimeter are nuclear interactions, which results in a hadronic shower in the detector. Since hadronic showers are longer than electromagnetic showers, they will deposit most their energy in the hadronic calorimeter. The hadronic showers however also include inelastic scattering with the nuclei in the detector, which means that there are more dominant processes than just bremsstrahlung and pair production. This means that even neutral hadrons will cause showers in the hadronic calorimeter.

Since muons are significantly more massive than electrons, they will only deposit a small fraction of their energy in the electromagnetic calorimeter, and unlike hadrons, they do not undergo nuclear interactions so they do not deposit as much energy in the hadronic calorimeter. Since muons are the only charged particles that do not cause significant showers, they are the only particles that reach and leave a trace in the muon tracker.

Invisible particles will pass straight through the detector without interacting with any of the layers. While they cannot be observed directly, their existence can be deduced using conservation of momentum. We know that the beam protons have $p_T = 0$, so the final state particles should also have $p_T = 0$ (in principle this is also true for the energy and the momentum along the beam axis, but this is difficult to measure since there will often be remnants of the protons that continue down the beam pipes instead of reaching the detector). If the measured p_T is not zero, it means that the missing p_T is carried by invisible particles that could not be seen in the detector. It is however in general not possible to tell how many invisible particles there are or where exactly they end up in the detector, it is only possible to know their total transverse momentum. In the Standard Model, the only particles that are fully invisible to the detectors are neutrinos, however in some dark sector models, such as Models E, SVJ and SVJL, some dark particles are expected to behave this way. It is not possible to tell if missing momentum in the detector is due to neutrinos or particles beyond the Standard Model.

4 Analysis

The previous chapters describe several different theoretical models that result in a wide range of possible dark matter signatures, as well as how experimental analysis at ATLAS works. This chapter will describe an analysis of simulation of these models in the ATLAS detector to arrive at a proposal for a generic definition of a dark jet.

4.1 Methodology

4.1.1 Monte Carlo samples

The analysis carried out in this thesis were performed using Monte Carlo simulated events generated using several general purpose event generators. Several file formats were used in this analysis as detailed in the following.

As Monte Carlo samples, we used several formats. For Models A-E, SVJ and SVJL, we used HEPMC files [21], which we generated ourselves using the Pythia event generator [19]. These files include complete parton level and particle level information, however, they do not include reconstruction level information. Pythia alone is also unable to accurately simulate emerging jets, so for the emerging jet models, we used the EVNT file format instead, provided using the ATLAS software [22]. The EVNT files include the same type of information as the HEPMC files, but were produced by others using tools that are more suitable for simulating emerging jets.

For all models, we also analyzed AOD files, which were also generated by the ATLAS software. These files contain particle level and reconstruction level information, however, their parton level information is very incomplete. This means that they are suitable for analyses involving the reconstruction level, but for analyses involving the parton level, the other formats had to be used.

4.1.2 Analysis tools

To analyze the HEPMC and EVNT files we used Rivet [23], and to analyze the AOD files we used the ATLAS 22.2.88 AnalysisBase software release with private code based on the xAOD framework [22].

The ATLAS AOD analysis can only be run on computers fully set up with the ATLAS software. We hence ran these analyses remotely on CERN's lxplus computer cluster. To do so, we used ROOT [24] in our xAOD code to produce .root files as an output, which we then locally converted into plots in the .pdf format using a small ROOT script.

To build the jets from at particle level, we used FastJet [25] with the anti-k_t algorithm. In Rivet, we used Rivet's `FastJets` class, which is a wrapper for FastJet taking Rivet particles as an input and outputting Rivet jets. For the particle level jets in the ATLAS xAOD code, we used a similar setup, though the code is a bit more complicated since we used FastJet without a wrapper.

For the reconstruction level jets in the ATLAS xAOD code, the jets themselves were included in the AOD files for some models but not for others. If they were directly available we used them directly, otherwise we constructed them using FastJet as described above, except using the reconstruction level tracks and energy deposits instead of the particle level ones.

4.2 Initial dark jet studies

Figures 4.1 and 4.2 show plots that display the "energy flow" of individual events for six different events in five different models.

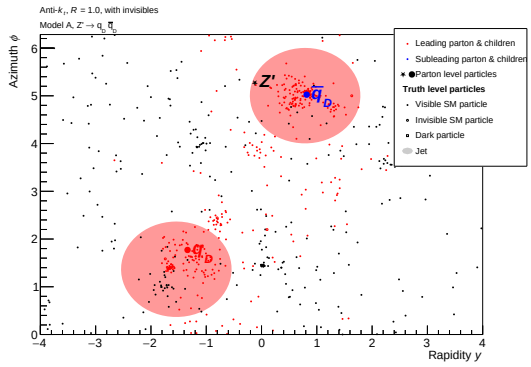

(a) Model A

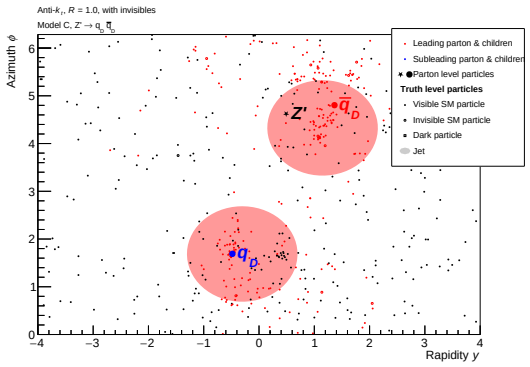

(b) Model C

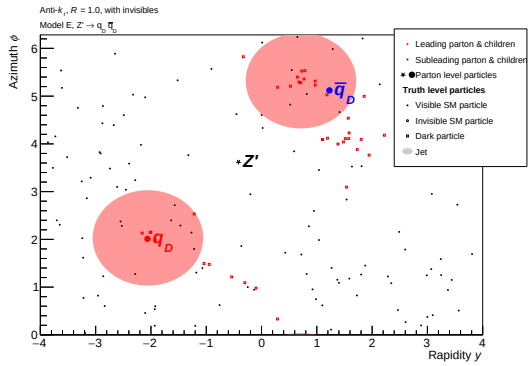

(c) Model E

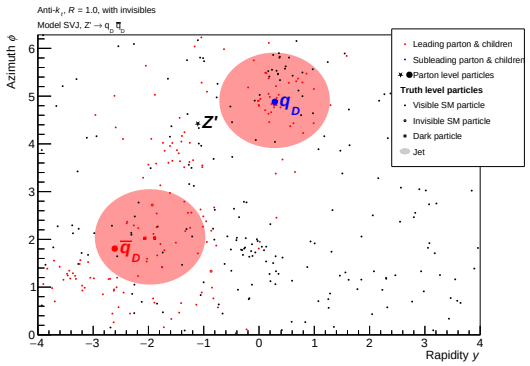

(d) Model SVJ

Figure 4.1: Representative event displays from four different models with a dijet topology. The two leading (highest p_{T}) jets are plotted in each case. In all cases, the two leading jets, which are built from stable particle level particles, also capture the two dark quarks within their extent in (y, ϕ)-space.

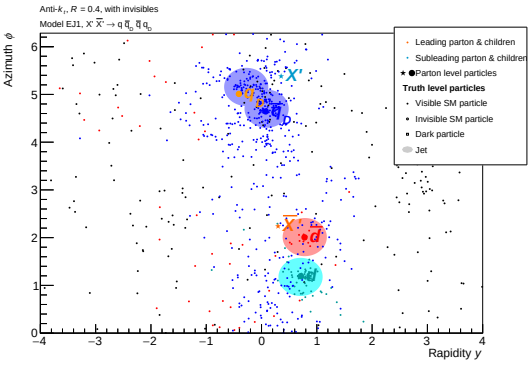

(a) X' boson decays directly into a dark quark and a Standard Model quark

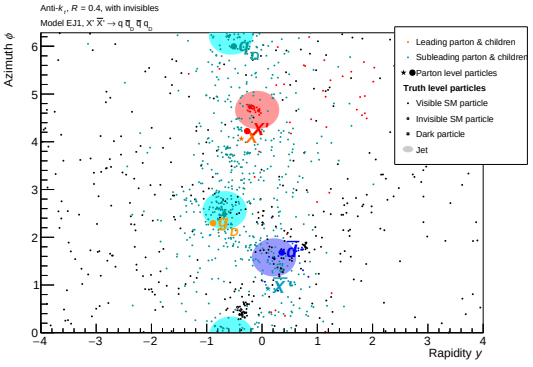

(b) X' boson emits a dark gluon

Figure 4.2: Event displays of two different events in Model EJ1, one where an X' boson radiates a dark gluon, one where the X' and anti-X' bosons both decay directly into a dark quark and a Standard Model quark. The four leading jets are plotted in each case.

We do not notice any major difference between Model A (Figure 4.1a) and Model C (Figure 4.1b). This is what we would expect, since the main difference between these models is that in Model A the dark mesons decay into Standard Model particles through the Z' boson, whereas in Model C this happens through the dark photon. This does not have any effect on the overall shape of the event, which is what we see here. The main difference between the Z' boson and the dark photon is that the dark photon couples to charged leptons, however, these plots do not differentiate between different types of visible Standard Model particles. We do not see any dark particles in the final state in these models, since the dark mesons decay into Standard Model particles very fast.

In Model E (Figure 4.1c), however, since the dark mesons are assumed to be stable in this model, we see that all non-background particles (in red) are dark particles (squares), and all Standard Model particles (circles) are background particles (black). Model SVJ (Figure 4.1d) is somewhere in between, we can see dark particles, but also non-background Standard Model particles.

What all models with a dijet topology have in common is that the parton level behaves the same way in all events in these models: the Z' boson decays into a dark quark-antiquark pair. However, in the models with a four jet topology, this is not the case. This is because as we can see in Figure 2.11, the X' boson has more Feynman diagram vertices that the Z' boson, allowing more processes to occur. The simplest such process is the one shown in Figure 2.12 where the X' bosons simply decay into a Standard Model quark and a dark quark each. However, it can also happen that the X' bosons radiate vector bosons prior to decay, most often dark gluons.

An example of this can be seen in Figure 4.2. Both plots show the same model (Model EJ1), but in one case the X' boson radiates a dark gluon prior to decay, whereas in the other case it decays directly into a dark quark and a Standard Model quark. In the models that we look at in this thesis, the X' boson has a greater coupling to the dark gluon than to Standard Model vector bosons, so it happens more often that the X' boson radiates a dark gluon than a Standard Model gluon, although the latter does happen. However, it almost never happens that the X' boson radiates an electroweak boson since the coupling is too small, although that is possible in theory.

In all models with a dijet topology (Figure 4.1), we notice that all particles originating from the Z' boson seem to originate from the same dark quark. However, this is due to technical limitations and is not relevant to the actual physics. This is because while the Z' boson is colorless, the dark quarks have dark color. This means that due to conservation of color, any dark quark-antiquark pairs created in the dark jets must get their color from both dark quarks (which they do through dark gluons), since the final state dark hadrons must be colorless. This means that even if one jet originated from one dark quark, the algorithm can still go back in the particle history in the MC event record through dark gluons and get to the other dark quark. In practice the same dark quark will always be chosen because the algorithm finds the parton by choosing the most energetic parent of each particle. So according to the MC event record all dark particles in these models originate from both dark quarks, but the algorithm needs to choose one.

In Model EJ1 (Figure 4.2), the dark particles behave similarly to the above. This is because just like the Z' boson, the Standard Model gluon that produced the $X'\bar{X}'$ pair carries no dark color. However, in the case of the Standard Model quarks, since the gluon itself is colored, there must be other (less energetic) particles around it that also have Standard Model color, so the gluon strings that formed the Standard Model jets can trace back through the particle history in the MC event record to those particles instead. Since the algorithm finds the parent parton by tracing back through the most energetic parents, it will often find the right parton in this case.

4.3 Choice of jet algorithm parameters

When building jets, there are several parameters that we must choose. These include the jet radius and which particles to include in the jets.

Code Snippet 4.1: Rivet code to define input particles and parameters of the jets.

```
const FinalState stableParticles;

/*Define the jet radius depending on the model. In practice this can
be implemented by passing parameters using environment variables.*/
const double jetRadius = modelHasFourJetTopology ? 0.4 : 1.0;

const FastJets jets(
    stableParticles,
    FastJets::ANTIKT,
    jetRadius,
    JetAlg::Muons::ALL,
    JetAlg::Invisibles::ALL
);
```

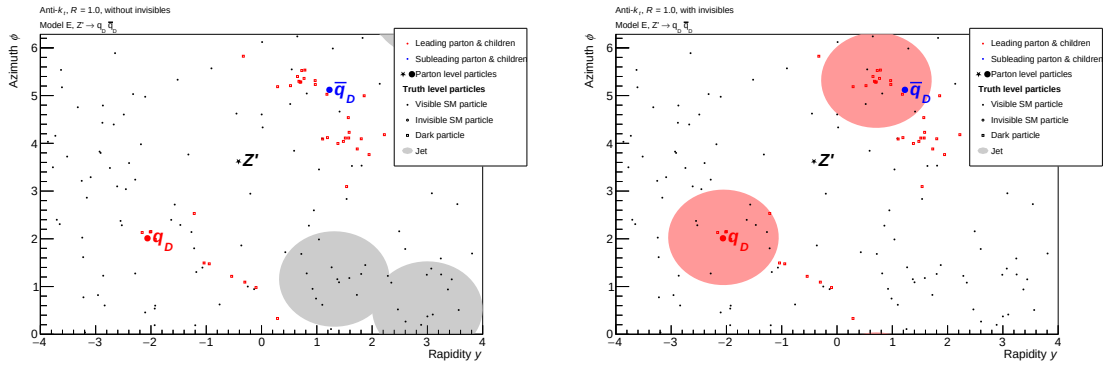

(a) Without invisibles

(b) With invisibles

Figure 4.3: Event display plots of the same event in Model E where invisible particles are included in the jet building of one but not the other. The two leading jets are plotted in each case.

4.3.1 Input particles to jet building

One important parameter when building jets is which particles to include. Often invisible particles are not included since they will not be visible at reconstruction level. However, in our case, not including invisibles can give incorrect results in models with high invisibility, since the jets will not include the particles we are interested in.

Particle level jets that include invisible particles better capture the parton level, while particle level jets that do not include invisible particles are more similar to reconstruction level jets. In other analyses, it is often useful to have jets that match the reconstruction level jets, in which case invisible particles would not be included. However, in our case, we want a particle level definition that works for any dark jet model, which means that it is better to include invisible particles. This will however have the disadvantage that the particle level jets will not always match the reconstruction level jets. We will have a closer look at how this can impact experimental searches in section 4.6.1.

A somewhat extreme example of where including invisible particles matters is Model E, where all interesting particles are dark particles and therefore invisible. As we can see in Figure 4.3a, if we build jets without invisible particles in Model E, the particle level jets will be completely unrelated

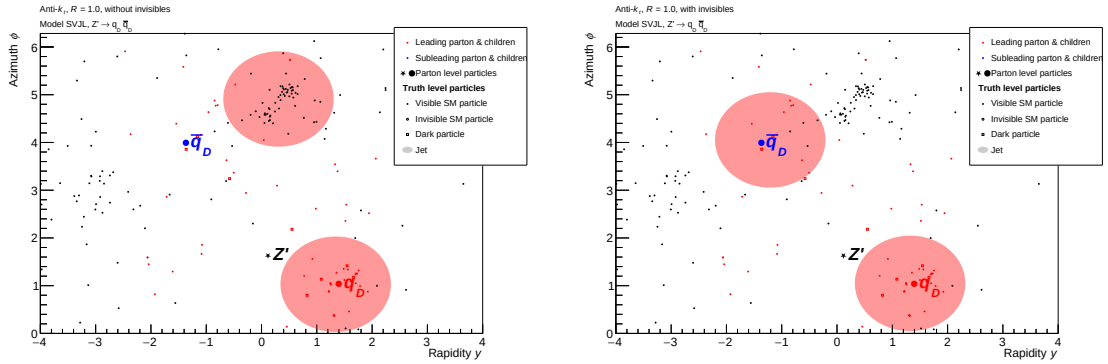

(a) Without invisibles

(b) With invisibles

Figure 4.4: Event display plots of the same event in Model SVJL where invisible particles are included in the jet building of one but not the other. The two leading jets are plotted in each case.

to the hard process involving the Z' boson. This can be compared with Figure 4.3b, which shows the same event but where invisibles were included in the jet building.

In Models SVJ and SVJL, not including invisible particles can also be an issue, though not as extreme. The particle level jets without invisibles in these models will often not be completely unrelated to the parton level since they will still capture the visible particles in the jet, but they will still fail to include a significant part of the jet. This can be seen in Figure 4.4, where one of the jets in Figure 4.4a is in the wrong place while still capturing some of the relevant particles. In Model SVJL this happens in a majority of events, while in Model SVJ, this only happens in a minority of events. This is due to Model SVJL having a higher invisible p_{T} fraction in the final state, as we will see in Section 4.6.1.

We will therefore include invisibles when building particle level jets. This ensures that our particle level definition of a dark jet produces useful results even for models where dark mesons are stable at detector scales.

4.3.2 Choice of jet radius

Another important parameter is the jet radius. As we will see, the optimal choice of jet radius depends on the model. This is because the models with a four jet topology produce four partons resulting in four main jets, whereas the models with a dijet topology only produce two main jets. The choice of jet radius will not impact the proposed definition.

In models with a dijet topology, such as Model A, choosing a too small jet radius can result in not all particles being captured. For example, in Figure 4.5, if we choose $R = 0.4$, the lower jet will be centered on a small cluster consisting mainly of background particles, ignoring most (but not all) of the particles originating from the dark quark that are more spread out. With $R = 1.0$, however, the jet correctly includes most of the particles originating from the dark quark. While this event is a somewhat extreme case in the fact that it actually focuses on the wrong area, it happens in quite a few events that many interesting particles are ignored if we choose a too small jet radius.

However, in models with a four jet topology, such as Model EJ1, choosing a too large jet radius can give the opposite problem. For example, in Figure 4.6, if we choose $R = 1.0$, most particles originating from both the d and $\bar{d}$ quarks will fit in the same jet, and the same is true for particles originating from the q_{D} and $\bar{q}_{\mathrm{D}}$ dark quarks. The two remaining jets will include mostly background particles and particles originating from any parton that get spread out. With $R = 0.4$, however,

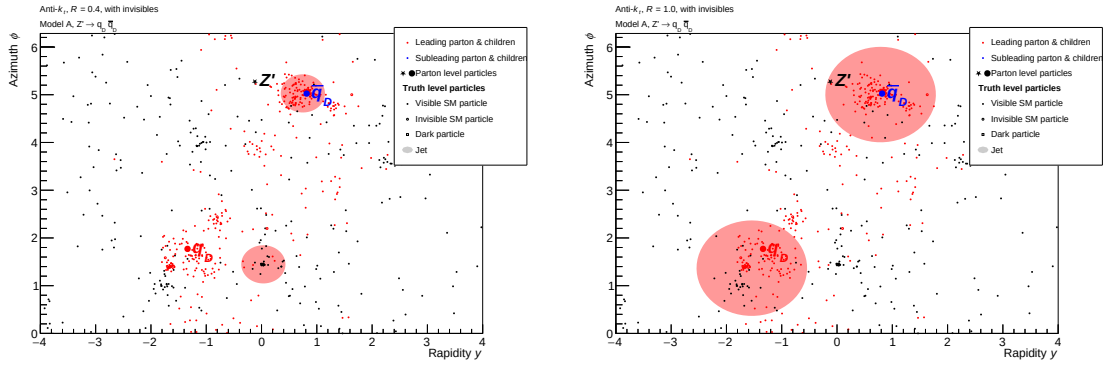

(a) $R = 0.4$ (b) $R = 1.0$

Figure 4.5: Event display plots of the same event in Model A with different values for the jet radius. The two leading jets are plotted in each case. Note that in most events this does not happen, this event was picked to highlight the issue.

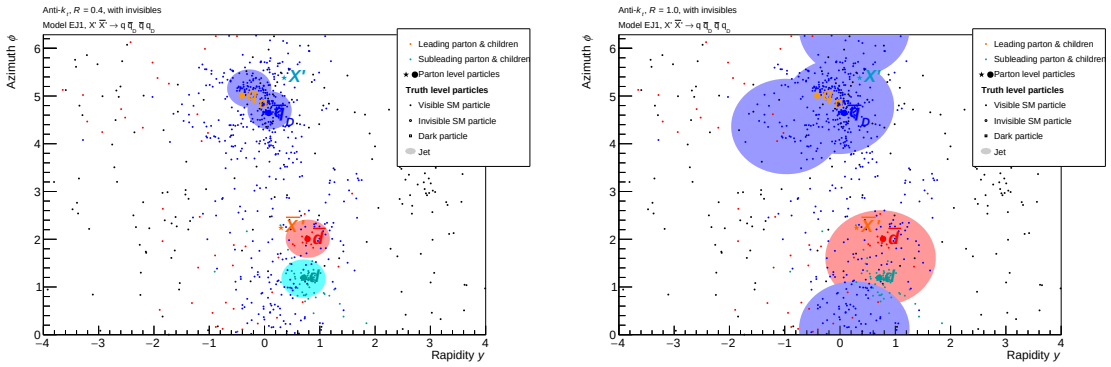

(a) $R = 0.4$ (b) $R = 1.0$

Figure 4.6: Event display plots of the same event in Model EJ1 with different values for the jet radius. The four leading jets are plotted in each case.

each jet correctly captures each parton.

In addition to looking at individual events, we can also make a more quantitative analysis by looking at three quantities: the *purity*, the *response* and the *efficiency*. In the following analysis, we will only consider the two leading jets in models with a dijet topology or the four leading jets in models with a four jet topology.

We define the purity $\mathcal{P}_{\text{jet}}$ and response $\mathcal{R}_{\text{jet}}$ of a jet (not to be confused with the jet radius R) with respect to a parton as:

$$\mathcal{P}_{\text{jet}} = \frac{1}{p_{\text{T}_{\text{jet}}}} \sum_c p_{\text{T}c} \tag{4.1}$$

$$\mathcal{R}_{\text{jet}} = \frac{p_{\text{T}_{\text{jet}}}}{p_{\text{T}_{\text{parton}}}}, \tag{4.2}$$

where c in equation (4.1) refers to constituents in the jet that originate from the parton. This means that the purity of a jet is the amount of its p_{T} that originates from the correct parton, and its response is how much of the p_{T} of the parton that we can find in the jet.

To find which parton matches which jet, for each jet, we select the parton that minimizes

Table 4.1: Purity, response and efficiency as a function of the model and the jet radius

Model and jet radius	Average purity	Average response	Efficiency
Model A, $R = 0.4$	0.50	0.77	0.85
Model A, $R = 1.0$	0.48	0.92	0.94
Model EJ1, $R = 0.4$	0.47	0.86	0.52
Model EJ1, $R = 1.0$	0.42	1.06	0.68

$\Delta R_{\text{parton,jet}}$ as defined in equation (3.3). We also require that no two jets share the same parton. If they would, the most energetic jet gets priority, and the following jets must select a parton that is not already used.

We can calculate the average purity $\langle \mathcal{P} \rangle$ and the average response $\langle \mathcal{R} \rangle$ by averaging $\mathcal{P}_{\text{jet}}$ and $\mathcal{R}_{\text{jet}}$ over all jets in all events:

$$\langle \mathcal{P} \rangle = \frac{\sum_{\text{jet}} \mathcal{P}_{\text{jet}}}{n_{\text{jets}}} \qquad \langle \mathcal{R} \rangle = \frac{\sum_{\text{jet}} \mathcal{R}_{\text{jet}}}{n_{\text{jets}}}, \tag{4.3}$$

where n_{jets} is the number of jets.

We can also define the efficiency $\mathcal{E}$ over all jets in all events as the fraction of jets that have a ΔR with the closest parton less than or equal to the jet radius R:

$$\mathcal{E} = \frac{n_{\text{match}}}{n_{\text{jets}}}. \tag{4.4}$$

where n_{match} is the number of jets where ΔR between the parton and the jet is less than R.

The average purity, the average response and the efficiency are shown in Table 4.1 for Models A and EJ1 with $R = 0.4$ and $R = 1.0$.

Ideally, in the general case (for any jets, not just for dark jets), we would want all three of these quantities to be 1. A purity of 1 would mean that all particles in the jet originate from the correct parton, a response of 1 means that the jet has no missing or excess p_{T} with respect to the parton, and an efficiency of 1 means that all partons are within the corresponding jet.

However, as we saw in the previous section, there is no way to tell which dark jet originates from which dark quark, since both dark jets can be traced back to both dark quarks through the dark gluons. This means that when calculating the purity, the algorithm will get half the particles wrong, which means that for dark jets specifically, the ideal purity would be 0.5 instead of 1.

It is clear that the purity will never be greater than 1 since the total p_{T} of all particles the jet is never smaller than the p_{T} of some particles in the same jet. It is also clear that the efficiency will never be greater than 1 since the number of jets with $\Delta R < R$ can never be greater than the total number of jets. The only one of these three quantities that can be greater than 1 is the response, which can happen if particles not originating from the parton are also included in the jet.

We expect the purity to decrease with an increasing jet radius, since increasing the jet radius will add particles that do not originate from the correct parton. The response will increase with the jet radius since the p_{T} of the jet increases with the jet radius, whereas the p_{T} of the parton stays the same. The efficiency will also increase with the jet radius since if R is greater, there are more values for ΔR that satisfy $\Delta R < R$.

In Table 4.1, we see that for Model A, the efficiency and response are the quantities that change the most, and both of them are better for $R = 1.0$. This is consistent with what we saw when analyzing Figure 4.5, where $R = 1.0$ seemed better. Therefore, for models with a dijet topology, we conclude that we will use a jet radius of $R = 1.0$. Figure 4.5 highlights the fact that the partons are outside the jet more often for $R = 0.4$ than $R = 1.0$, which means that the efficiency is smaller for a smaller jet radius. If we look at the last column in Table 4.1, we see that the efficiency is

85% for $R = 0.4$ and 94% for $R = 1.0$, which means that issues similar to the one in Figure 4.5 happen in about $94\% - 85\% = 9\%$ of events.

For Model EJ1, the difference in purity between $R = 0.4$ and $R = 1.0$ is larger than in Model A. This is consistent with what we saw in Figure 4.6, where two of the four jets include both partons and therefore include particles from both of them, and the two other jets are not centered around any of the partons and therefore include background particles. The response is smaller than unity for $R = 0.4$ and larger than unity for $R = 1.0$, so none is significantly better than the other. The efficiency is significantly smaller than unity in both cases. One explanation for this could be that when a dark gluon is emitted, the algorithm will try to calculate the efficiency between one of the jets and the X' boson after it has emitted a gluon but before it has decayed into dark quarks. This is visible in Figure 4.2b, where we can see that the red X' boson is slightly outside of the red jet. There are other events where this is more extreme and the X' boson is very far out of the jets.

This means that if we prioritize the purity, we should select $R = 0.4$, whereas if we prioritize the efficiency, we should select $R = 1.0$. For the response, both values of R are acceptable. Since the efficiency is bad no matter what whereas the purity is quite good for $R = 0.4$ (considering the fact that the ideal purity for dark jets is 0.5), we choose to prioritize the purity by choosing to use $R = 0.4$ in models with a four jet topology. This is also consistent with Figure 4.6, where $R = 0.4$ is clearly a better choice.

This means that in models with a dijet topology (Models A-E and SVJ), we will use $R = 1.0$, whereas in models with a four jet topology (Models EJ1-EJ4), we will use $R = 0.4$. In order for our analysis to work well even in models like Model E (and to a lesser extent Models SVJ and SVJL), we choose to include invisible particles when building particle level jets. The code for building such jets in Rivet is shown in Code Snippet 4.1.

4.4 Proposed dark jet definition

The previous sections have presented studies that resulted in a suitable definition of particle level jets. The next step is to arrive at a technical definition of how to judge if a given such jet is dark or not, and how to determine key properties of these jets.

4.4.1 Motivation

In addition to particles originating from dark particles, all events also have background particles which originate from purely Standard Model processes. The particle level jets, which contain many tens of particles, will hence essentially never be fully dark (where by "dark" we mean originating from dark particles). Since in some models the dark mesons decay into Standard Model particles, we would like a definition that can tell whether a jet mainly originated from dark particles, regardless of whether the final state particles are Standard Model particles or dark particles. For example, the jets in Models A and C shown in Figure 4.1a and 4.1b should be considered dark jets even though they only contain Standard Model particles, because those particles originate from dark particles. Jets in Model E, Model SVJ or Model SVJL that consist of dark particles in the final state should also be considered dark jets.

Models with a dijet topology should therefore most often have two high-energy dark jets and no high-energy Standard Model jets (i.e. non-dark jets), since the Z' boson decays into two dark quarks. Models with a four jet topology should most often have two high-energy dark jets and two high-energy Standard Model jets, since the X' boson and the anti-X' boson decay into one dark quark and one Standard Model quark each, resulting in a total of two dark quarks and two Standard Model quarks. However, since the X' boson can easily radiate dark gluons as seen in Figure 4.2b, it is acceptable if these models have a significant number of events with more dark

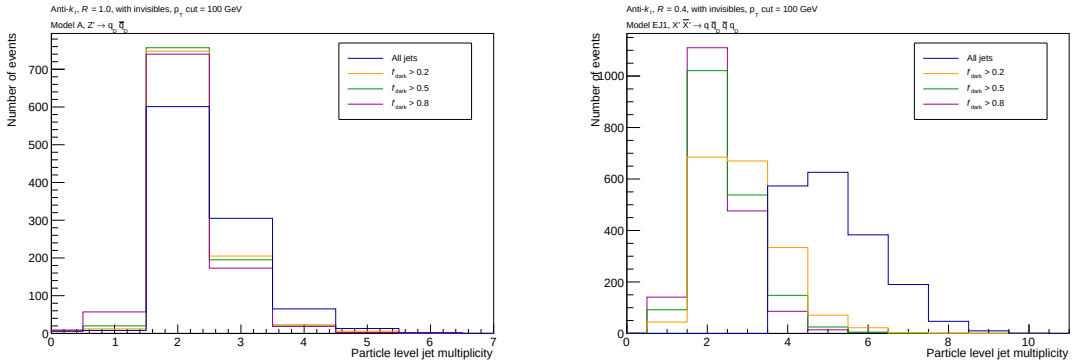

(a) Model A

(b) Model EJ1

Figure 4.7: Jet multiplicity distributions of Models A (left) and EJ1 (right) for jets with $p_T \geq 100\,\text{GeV}$ and different darkness criteria. For both these models, we expect a topology of two dark jets, each with $p_T \approx 500\,\text{GeV}$, and occasionally additional dark jets due to wide angle radiation.

jets. Even in models with a dijet topology it is possible for the dark quarks to radiate dark gluons (although the Z' boson itself cannot do that), so even in those models it is acceptable to have a few events with more than two dark jets.

At the particle level, we have access to the ancestors of each particle through the MC event record, so it is reasonable to have a definition where we directly look at these ancestors. Since a dark jet may contain low-energy background particles without dark ancestors, we cannot require a dark jet to contain 100% particles with dark ancestors. Similarly, it is possible that individual particles leave the dark jet (for instance through a decay), so it is not enough to require that a dark jet contains at least one particle with dark ancestors. For these reasons, we will require that at least a certain percentage of the jet has dark ancestors for it to be considered a dark jet.

In most models, dark particles interact with each other less than Standard Model particles, which means that before the dark mesons decay into Standard Model particles, there will be fewer dark particles than background Standard Model particles. However, since they originate from the very massive portal bosons, they will be more energetic. This means that for our definition to give useful results in models like Model E, Model SVJ or Model SVJL where dark mesons are stable at detector scales, we need to look at how much p_T of the jet originates from dark particles rather than how many individual particles.

To judge if a jet is dark or not, we define the quantity *darkness* as the fraction of p_T carried by jet constituent particles that either are dark or have dark ancestors:

$$f_{\text{dark}} = \frac{p_{T\,\text{dark}}}{p_{T\,\text{jet}}}, \tag{4.5}$$

where $p_{T\,\text{dark}}$ is the total p_T of particles in the jet that have dark ancestors. In Figure 4.7, we plotted the number of jets that have have at least 80% of their p_T originating from dark particles (purple line), at least 50% (green line), at least 20% (orange line), as well as the total number of jets regardless of darkness (blue line). In each case, we only counted jets with $p_T \geq 100\,\text{GeV}$ in order to avoid low-energy background jets. In Figure 4.7, only Models A and EJ1 are shown because the plots for all models with a dijet topology look very similar to Model A and the plots for all modes with a four jet topology look very similar to Model EJ1.

In Model A (Figure 4.7a), it does not make any significant difference if we choose a darkness criterion of 20%, 50% or 80%. 80% is slightly better for avoiding too many jets, whereas 20% is slightly better for avoiding having only one jet. However, the difference is negligible, so any of

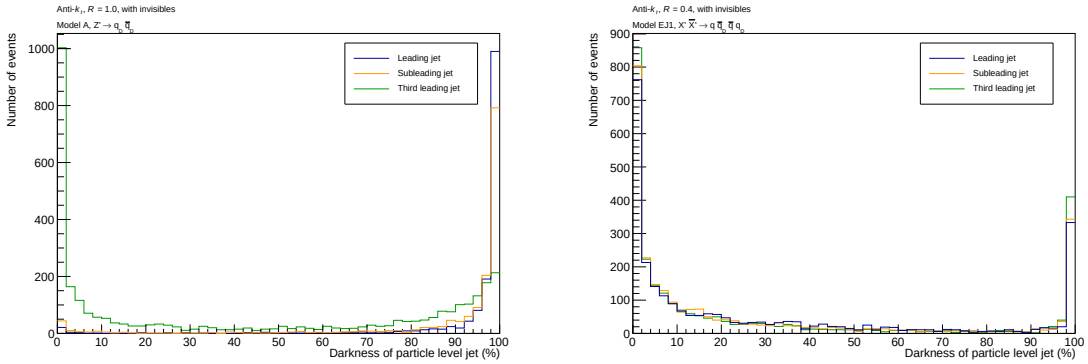

(a) Model A

(b) Model EJ1

Figure 4.8: Darkness distributions of the three leading jets.

those criteria can be used for Model A.

In Model EJ1 (Figure 4.7b), however, we see that requiring a larger darkness is better. If we only require $f_{\text{dark}} > 20\%$ we often get too many jets, whereas with 80% we often get the desired outcome.

The reason why the difference is larger here than in Model A is most likely because there are more jets, meaning that they will be closer together leading to a higher probability that particles from one jet end up in the other jet. For example, if we look at Figure 4.2b, we can see that the blue jet originating from the Standard Model anti-down quark contains many particles in cyan, meaning they originate from either the dark gluon or the dark quark (it is not possible to tell which due to the issue described in the previous section). This is most likely due to the fact that the jet originating from the down quark is relatively close to the one originating from the dark gluon. This can be contrasted with the models with a dijet topology shown in Figure 4.1, where, despite the larger jet radius, the jets are farther away from each other since there are only two of them emitted back to back. So in this case, defining a dark jet as a jet with at least 80% of its p_{T} originating from dark particles seems reasonable.

We can also look at how many jets have a given darkness. Figure 4.8 shows the number of events where the leading jet (blue), the subleading jet (orange) and the third leading jet (green) have a given darkness. Again, this is shown for Model A, which has a dijet topology, and Model EJ1, which has a four jet topology.

In Model A (Figure 4.8a), we see that the two leading jets have very high darkness, whereas the third leading jet often has very low darkness. This is expected, since this model should only have two main jets that are both dark jets, meaning that the third leading jet is a background Standard Model jet.

We see that in Model A the two leading jets very rarely have a darkness less than 80%. The third leading jet often has a darkness close to zero, then intermediate darkness becomes more rare, then for high darkness it increases again. The majority of events where the third leading jet has a very low darkness are most likely events where the third leading jet is a background Standard Model jet. The events where the third leading jet has an intermediate darkness are probably also events where the third leading jet is a background jet, but where high energy dark particles have left the dark jet and ended up in the background jet, which means that we do not want to count those as dark jets. The events where the third leading jet has a high darkness are most likely events where a dark quark has radiated a dark gluon that formed its own jet, so we want to count those as dark jets. Since the green curve starts increasing around 80%, this means that defining a dark jet as a jet with at least 80% darkness seems reasonable in this case as well.

In Model EJ1 (Figure 4.8b), we do not see any noticeable difference between the three leading jets, which makes sense because this model has four main jets with similar p_{T}. All three curves have two peaks, one at 0% darkness and one at 100% darkness, which makes sense because in this model, half the main jets are dark jets and half of them are Standard Model jets. We see that the curves have a minimum around 80% darkness, which makes that a good point to separate the Standard Model jets to the left from the dark jets to the right. So requiring the darkness to be at least 80% in the definition of a dark jet makes sense here as well.

4.4.2 Definition

For the reasons mentioned in the previous section, our proposed definition of a dark jet is a jet with at least 80% of its p_{T} originating from dark particles.

This definition is implemented in four different functions. The first one checks if a given particle is a dark particle by comparing the absolute value of its PDG ID towards a regular expression. The PDG ID is a number unique for each particle type that is used by simulation and analysis software to keep track of which particle has which type. The PDG IDs of Standard Model particles can be found in Ref. [26], and the PDG IDs of particles beyond the Standard Model used in this thesis can be found in Table 2.2. In most models, including all the models used in this thesis, the default regular expression `^490[0-9][1-9][0-9]{2}$` matches the desired PDG IDs. This requires the first three digits in its PDG ID to be `490` (which is used by most models to denote particles related to the dark sector), but requires its third digit from the end to be non-zero in order to exclude portal bosons. This second restriction is especially important in models with a four jet topology, where the X' boson decays into a dark quark and a Standard Model quark, since we do not want the jet originating from the Standard Model quark to be considered dark.

For models that use different PDG ID conventions, it is possible to override this with a custom regular expression by setting the `DARK_REGEX` environment variable.

The second function loops over the particle history in the MC event record to assert if a given particle has a dark ancestor. To do this, it starts with a final state particle and asserts if that particle is dark using the function defined before. If it is, it returns true, otherwise, it looks at the most energetic parent of that particle and checks if that one is dark, and so on until it either finds a dark particle and returns true, or a particle with no parents (often the beam protons) and returns false.

The reason why this function only checks the most energetic parent of each particle rather than all parents is for performance. Since this function needs to be run over millions of particles, it needs to be fast. While this can give a few false negatives in some rare cases, overall it works well as we will see in the next section.

The third function calculates what fraction of the p_{T} of a jet originates from dark particles. The implementation of this is fairly straightforward, it loops over all particles checking if it has a dark ancestor, if it does it adds its momentum to the result, then finally extracts the p_{T} from the momentum and normalizes the result by dividing by the total p_{T} of the jet. To avoid rare occurrences of $f_{\mathrm{dark}} > 1$ that can happen due to limited numerical precision, the darkness calculation is capped at unity. This only happens very rarely and when it does happen the error is very small, but in some cases it can be useful for downstream code to assume that the returned value is exactly between 0 and 1.

Finally, the fourth function checks if the jet should be considered a dark jet according to this definition by comparing the value returned by the previous function with 0.8.

A Rivet implementation of this is provided in Code Snippet 4.2. A full implementation of these methods and associated Rivet algorithms is provided in Ref. [27].

Code Snippet 4.2: Rivet code implementing the proposed particle level definition of a dark jet. Note that it is assumed that the jet is built including invisible particles as detailed in Code Snippet 4.1.

```
static bool particleIsDark(const Rivet::Particle &particle){
    static const std::regex darkParticleRegex(
        getStringFromEnvVar(
            //Allow to override dark regex by setting an environment variable
            "DARK_REGEX",
            //Default regex that matches PDGIDs of dark particles
            std::string("^490[0-9][1-9][0-9]{2}$")
        )
    );
    return std::regex_search(
        std::to_string(particle.abspid()),
        darkParticleRegex
    );
}

static bool hasDarkAncestor(Rivet::Particle particle){
    if(particleIsDark(particle)){
        return true;
    }
    while(particle.parents().size() > 0){
        particle = particlesByEnergy(particle.parents())[0];
        if(particleIsDark(particle)){
            return true;
        }
    }
    return false;
}

static double pTDarkness(const Rivet::Jet &jet){
    Rivet::FourMomentum momentum;
    for(const Rivet::Particle &particle: jet.particles()){
        if(hasDarkAncestor(particle)){
            momentum += particle.momentum();
        }
    }
    return std::min(momentum.pT() / jet.pT(), 1.0);
}

//Method to judge if a jet is dark. The default, recommended cut is 80%.
//Note that jet should be built including invisible particles.
static bool jetIsDark(const Rivet::Jet &jet, double darknessCut = 0.8){
    return pTDarkness(jet) >= darknessCut;
}
```

4.5 Validation of the proposed dark jet definition

This section presents an analysis that investigates performance of the dark jet definition that was established in the previous section. To do this, we will look at how different observables behave when we require that jets are dark according to our definition.

4.5.1 Jet multiplicity

The easiest way to test our definition is to count how many jets are dark according to this definition. Figure 4.9 shows the total number of jets with $p_{\mathrm{T}} \geq 100\,\mathrm{GeV}$ for several models with both a dijet and a four jet topology. Figure 4.9a shows the models with a dijet topology, and Figure 4.9b shows the models with a four jet topology. These figures do not use our definition, but are a good place to start to make sure that the results are what we expect before using our definition.

We see in Figure 4.9a that for the models with a dijet topology, the jet multiplicity peaks at two or three jets. Two jets is expected, and three jets is also possible, either if one of the dark quarks radiates a dark gluon or if there is a background jet with enough p_{T}. It can also happen in some cases that there are four jets if two background jets have enough p_{T}. However, as expected, it is very rare to have fewer than two jets.

In Figure 4.9b, we see that for models with a four jet topology, the multiplicity peaks at five jets. If the X' bosons decay directly into a dark quark and a Standard Model quark, four jets are expected, however, as we saw before, the X' boson can also radiate dark gluons or Standard Model gluons, which explains why it is more frequent to have more than four jets.

Now that we have looked at how many jets there are in total in each model, we can apply our definition to count how many of those jets are dark jets (with $f_{\mathrm{dark}} \geq 0.8$) and how many are Standard Model jets (with $f_{\mathrm{dark}} < 0.8$). In models with a dijet topology, we see in Figure 4.10a that the peak at two jets is more pronounced, and we see in Figure 4.11a that there is a peak at 0-1 Standard Model jets. This is expected since these models should have two main jets originating from the Z' boson and the dark quarks, and the other jets are often Standard Model background jets. We can see in Figure 4.10a that there are sometimes three dark jets, which corresponds to cases where a dark quark radiates a dark gluon, but very rarely more than three dark jets.

In Figure 4.10b, for models with a four-jet topology, we see that there is a clear peak at two dark jets for all models except Model EJ3 where there is a peak at three dark jets. A peak at two dark jets with a large number of events with three dark jets is expected since the X' boson and the anti-X' boson each decay into one dark quark, resulting in a total of two dark jets, and the X' or anti-X' boson can sometimes radiate a dark gluon, which would produce an additional dark jet.

The only of these models that has more dark jets than the others is Model EJ3. In Table 2.4, we can see that in Model EJ3, the dark mesons are more massive than in the other models, and decay into relatively light Standard Model down quarks. This would mean that when the dark mesons in a dark jet decay, the jet can sometimes separate into two jets due to the decay products having large opposite momentum. This could explain why there are more dark jets in Model EJ3 than in the other models. This is consistent with the result from Ref. [28], where the ΔR between two jets resulting from a decay is proportional to the mass m of the particle that has decayed:

$$\Delta R \approx \frac{2m}{p_{\mathrm{T}}} \tag{4.6}$$

In Figure 4.11b, we see a peak at two Standard Model jets for all models, with a significant number of events having three Standard Model jets. The X' boson decays into a Standard Model quark and the anti-X' boson decays into a Standard Model antiquark, which results in a total of two Standard Model jets. The additional jets can either be background jets or come from the X' or anti-X' boson emitting a Standard Model gluon.

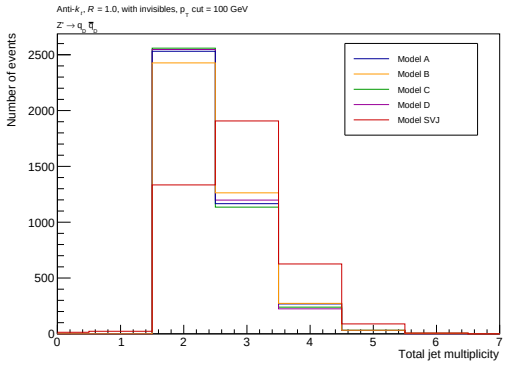

(a) Models A-D and SVJ

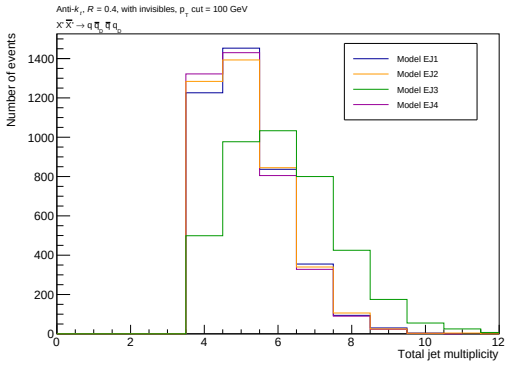

(b) Models EJ1-EJ4

Figure 4.9: Multiplicity of jets with $p_{\mathrm{T}} \geq 100\,\mathrm{GeV}$ for the dark sector models under investigation. The dark dijet resonance models (left) have two jets at tree level, while the emerging jet models (right) have four jets at tree level, however, all models can have additional jets due to final state radiation.

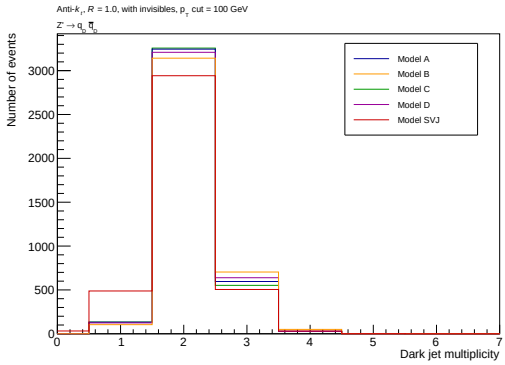

(a) Models A-D and SVJ

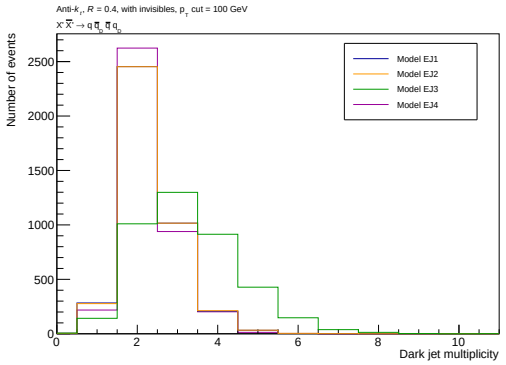

(b) Models EJ1-EJ4

Figure 4.10: Multiplicity of jets with $p_{\mathrm{T}} \geq 100\,\mathrm{GeV}$ and $f_{\mathrm{dark}} \geq 0.8$ for the dark sector models under investigation.

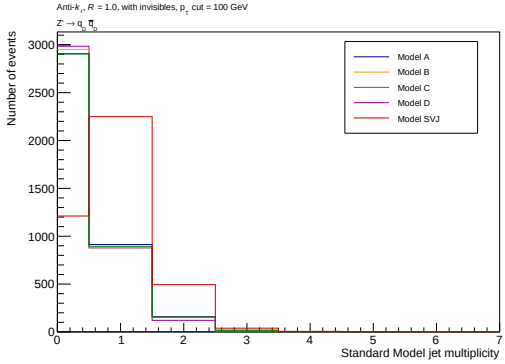

(a) Models A-D and SVJ

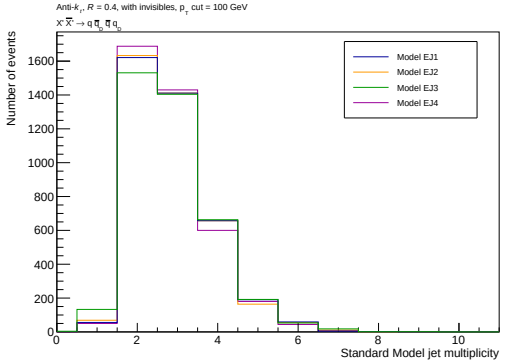

(b) Models EJ1-EJ4

Figure 4.11: Multiplicity of jets with $p_{\mathrm{T}} \geq 100\,\mathrm{GeV}$ and $f_{\mathrm{dark}} < 0.8$ for the dark sector models under investigation.

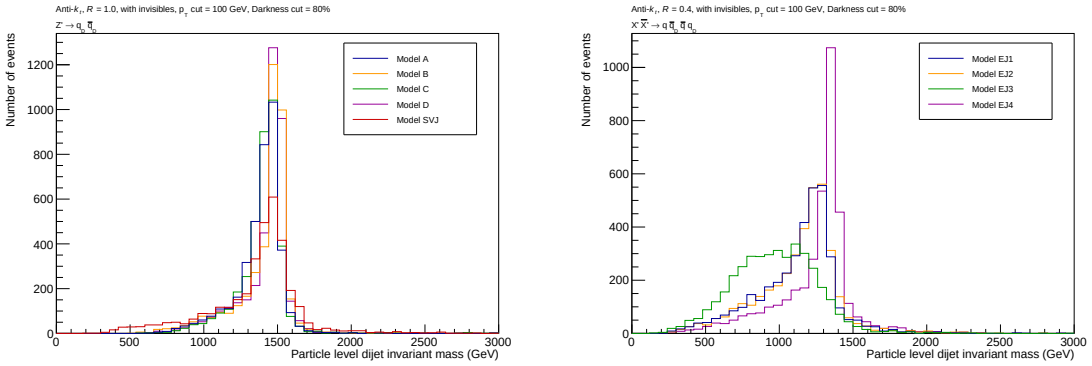

(a) Models A-D and SVJ

(b) Models EJ1-EJ4

Figure 4.12: Dijet invariant mass of the two jets that should originate from the portal boson (Z' or X'). In Models A-D and SVJ, these are the two leading dark jets. In Models EJ1-EJ4, these are selected by pairing a dark jet with a non-dark jet.

4.5.2 Dijet invariant mass

Another way to validate the performance of our dark jet definition is to investigate the dijet invariant mass. If we manage to correctly select the two jets that originate from the dark portal boson, the associated dijet invariant mass should be close to that of the portal boson.

For models with a dijet topology, this is fairly straightforward. Since the Z' boson decays into two dark quarks, we select the two dark jets with highest p_{T} and calculate their invariant mass. This invariant mass should peak at 1500 GeV, since that is the mass of the Z' boson in all the models we look at. In Figure 4.12a, we see that this invariant mass does peak at 1500 GeV as expected, so our definition works well in this case.

For models with a four jet topology, however, this is more complicated. In these models, we expect to have two dark jets and two Standard Model jets, so we start by selecting the two dark jets with highest p_{T} and the two Standard Model jets with highest p_{T}. We then need to find out which of the two dark jets and which of the two Standard Model jets originated from the same X'/anti-X' boson. There are two different ways to pair each dark jet with a Standard Model jet, and we pick the one that gives the most similar dijet invariant mass. We then expect the dijet invariant mass of each pair to peak around 1400 GeV, since that is the mass of the X' boson in the models we use.

The result of this is shown in Figure 4.12b. We see that all models except Model EJ3 have a clear peak around 1400 GeV as expected. They also have a tail at lower masses, but very rarely have higher masses. This is expected, since energy can be lost to a third jet in cases where an on-shell X' boson radiates a gluon (dark or Standard Model), becomes off-shell and then immediately decays into a Standard Model quark and a dark quark. However, there is no similar process that could increase the dijet invariant mass, which explains why the tail is only to the left and not to the right.

In Model EJ3, however, the peak is around 1000 GeV instead, but is not sharp at all. This is consistent with what we saw in the previous section, that there are more jets in Model EJ3 than in the other models, most likely due to the the dark mesons and dark quarks being significantly more massive. Since there are more jets, the energy resulting from the mass of the X' boson is spread across more jets, which means that only considering two of those jets will result in a peak at a lower mass. Since Model EJ4, which has very light dark mesons, has a sharper peak at 1400 GeV than Models EJ1 and EJ2, this confirms the hypothesis that a higher dark meson mass leads to more jets. This can also be seen to a lesser extent in Figure 4.12a, where Models B and

D, which have lighter dark mesons, have a sharper peak at 1500 GeV.

The fact that Figure 4.12b looks reasonable is especially good for our definition, since pairing the jets correctly is important to be able to get back the correct mass. Since we used our definition to require that dark jets must be paired with Standard Model jets and got a reasonable result, this means that our definition for which jets are dark jets and which ones are Standard Model jets works well. This can be compared to Figure 4.16b, which is a similar plot but where we simply chose the two leading jets without using our definition. The fact that the one where we did use our definition looks better means that our definition works well in this case.

4.6 Suggestions for experimental analyses

We have settled on a particle level definition that captures the parton level topology. We can define dark and Standard Model (non-dark) jets. However, these dark jets can have different properties that make them manifest quite differently at detector level. This section introduces a set of quantities that can be calculated at particle level to define a specific dark jet signature suitable for experimental analysis.

4.6.1 Invisibility

Some models, such as Model E, Model SVJ and Model SVJL, have dark hadrons that are stable at detector scales. These do not leave detector signals, and are hence referred to as invisible. A feature of dark jets produced by said models is a high fraction of such invisible particles, which is quantified by a quantity called *invisibility*.

In the Standard Model, neutrinos are invisible and will give rise to missing p_{T} as described in section 3.2.2. If we were to just look at one event, there is no way of distinguishing between neutrinos and dark particles since both would go straight through the detector without leaving any trace. However, since neutrinos are part of the Standard Model, their production cross section at the LHC is well known, so it is possible to calculate how much missing energy there should be on average in Standard Model jets due to neutrinos alone. This has been simulated before by others and is well-known: as we can see in Figure 4.13, it is so small that it does not even have its own label, and is instead included in "rest". This is because since neutrinos do not hadronize, they are rarely present in jets, even though their presence in itself is nothing unusual. This means that if many jets with a high amount of missing energy are observed, it may be evidence for dark matter.

To see how the different dark QCD models behave with respect to invisibility, we can look at the invisibility of the particle level jet as shown in Figure 4.14a, defined as

$$f_{\mathrm{inv}} = \frac{p_{\mathrm{T}_{\mathrm{inv}}}}{p_{\mathrm{T}_{\mathrm{jet}}}}, \tag{4.7}$$

where $p_{\mathrm{T}_{\mathrm{inv}}}$ is the amount of p_{T} at particle level carried by invisible particles, and $p_{\mathrm{T}_{\mathrm{jet}}}$ is the particle level p_{T} of the jet. This quantity is very similar to the r_{inv} observable presented in Ref. [29], with the difference being that f_{inv} is p_{T}-weighted.

We cannot make this plot at the reconstruction level since the reconstruction level does not include invisible particles. Table 4.2 shows the breakdown of this invisibility by type of invisible particle.

As expected, we see in both Figure 4.14a and Table 4.2 that the models with stable dark mesons (Models E, SVJ and SVJL) has higher invisibility than Models A-D, which do not have stable dark mesons. As we can see in Table 4.2, Model E has the highest invisibility since all dark mesons in that model are stable, followed by Model SVJL and then Model SVJ. The reason Model SVJL has a higher invisibility than Model SVJ is because according to Table 2.3, the $\pi_{\mathrm{D}}^{\text{“0”}}$ has a higher

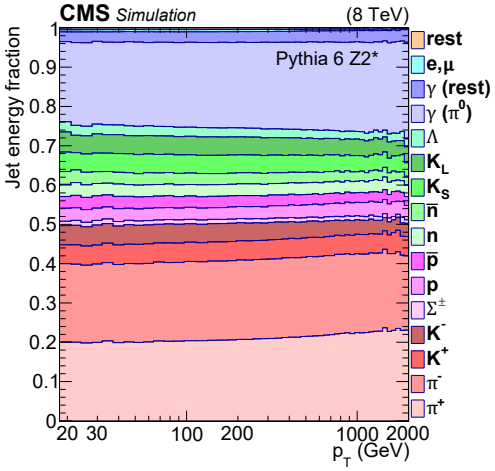

Figure 4.13: Particle distribution in Standard Model jets. Leptons and invisible particles are very rare in Standard Model jets, unlike in dark jets in some models. Source: [7]

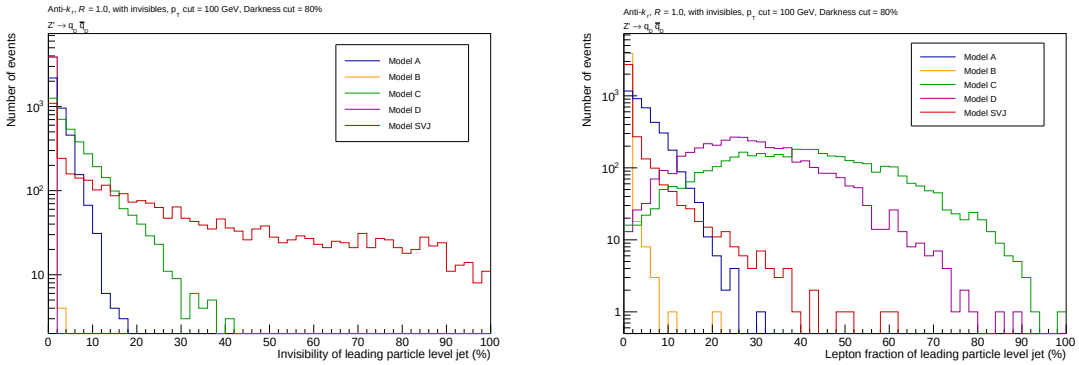

(a) Invisibility

(b) Lepton fraction

Figure 4.14: Percentage of p_{T} of the leading dark particle level jet carried by invisible particles or leptons in different models with a dijet topology.

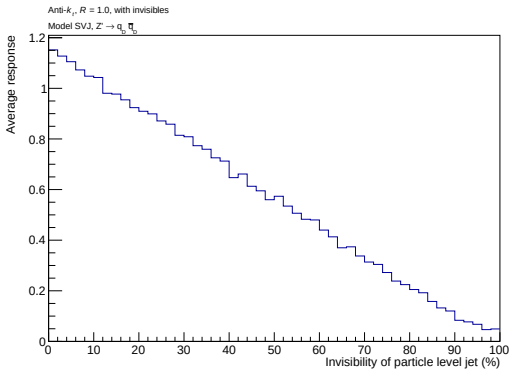

Figure 4.15: Response of the reconstruction level jet with respect to the particle level jet as a function of invisibility in Model SVJ.

Table 4.2: Average p_{T}-fraction of different invisible particles in different models with a dijet topology.

Particle	Model A	Models B, D	Model C	Model E	Model SVJ	Model SVJL
Neutrinos	2.2%	0.1%	4.8%	0.1%	1.1%	0.1%
$\pi_{\mathrm{D}}^{\text{“0”}}$	-	-	-	51.2%	-	-
$\pi_{\mathrm{D}}^{\text{“}\pm\text{”}}$	-	-	-	30.0%	4.6%	11.3%
$\rho_{\mathrm{D}}^{\text{“}\pm\text{”}}$	-	-	-	-	11.8%	34.6%
Total	2.2%	0.1%	4.8%	81.3%	17.5%	46.0%

branching ratio into stable dark mesons in Model SVJL than in Model SVJ. While the opposite is true for the $\rho_{\mathrm{D}}^{\text{“0”}}$, the difference between the two models is larger for the $\pi_{\mathrm{D}}^{\text{“0”}}$.

In Figure 4.14a, Model SVJ still has a peak at low invisibilities since the dark mesons have a high branching ratio into Standard Model particles, but it is the only model in Figure 4.14a that also has events at very high invisibilities.

Models A and C also have a relatively high invisibility, although it is not as high as in Model SVJ. Since dark mesons have a very short lifetime in these models, the invisible particles here are not dark particles, but neutrinos, as we can see in Table 4.2. This is expected since in Model A the dark mesons decay into Standard Model charm quarks, which themselves decay into neutrinos among other particles. Similarly, in Model C, as we can see in Table 2.5, the dark photon can decay into tau leptons and charm quarks, both of which decay into neutrinos among other particles.

As we can see with Models A and C, an excess of missing energy is not necessarily due to dark particles themselves, but can also be due to Standard Model neutrinos being produced through a process involving unstable particles beyond the Standard Model. This means that if we discover missing energy significantly greater that that predicted by the Standard Model, it does not automatically mean that we discovered dark matter, but rather some new physics that somehow produces many invisible particles that could be dark matter, neutrinos or something else.

We can also look at how the reconstruction level jets behave with respect to invisibility by using the response between particle level and reconstruction level. This is defined similarly to the response in equation (4.2), except that we divide the p_{T} of the reconstruction level jet by the p_{T} of the particle level jet.

We can then plot this response as a function of f_{inv} as shown in Figure 4.15. This plot can be made for any model, however, most models studied in this thesis have no events whatsoever with large values f_{inv}, so those models would have missing data points. Model SVJ is the only model with jets that cover all ranges of f_{inv}, so this is the most suitable one to plot.

We can see in Figure 4.15 that the response is a linear function of the invisibility, where jets with a low invisibility have a high response and vice-versa. This is expected since the detector cannot see invisible particles, which means that jets with a high f_{inv} will appear to be very soft to the detector as most of the jet will be invisible.

4.6.2 Lepton fraction

Unlike invisible particles, all leptons are part of the Standard Model, so their presence in itself is nothing unusual. However, since they do not hadronize, they are not very common in Standard Model jets, although they do exist. The most common source of leptons in Standard Model jets is the $\pi^0 \to e^+e^-\gamma$ decay mode, followed by decays of mesons containing charm and bottom quarks. However, since this is not the primary decay mode of the π^0 (which is $\pi^0 \to \gamma\gamma$), they are still quite rare in Standard Model jets. This can be seen in Figure 4.13: the lepton fraction, which is

the fraction of electrons and muons, is so small in Standard Model jets that it is hardly visible. So while leptons themselves are quite common (they can easily be produced through non-QCD processes), they are rare in Standard Model jets.

However, in some dark QCD models such as Models C and D, this is different. As we can see in Table 2.5, the dark photon has a branching ratio of around 30% into electrons and muons in both models, which is relatively high and will cause the jets to contain relatively many leptons (tau leptons are different since they can decay into hadrons). This means that a high lepton fraction in jets could be an indication for dark QCD, or at least some process beyond the Standard Model.

We can define the lepton fraction of a jet as

$$f_\ell = \frac{p_{\mathrm{T}\,\ell}}{p_{\mathrm{T\,jet}}}, \tag{4.8}$$

where $p_{\mathrm{T}\,\ell}$ is the total p_{T} of all leptons in the jet.

Figure 4.14b shows the lepton fraction of the leading dark jet in the five models with a dijet topology. As expected, Models C and D have a very high lepton fraction due to the decay of the dark photon. The reason why Model C has a higher lepton fraction than Model D is most likely because in Model C the dark photon can decay into tau leptons and charm quarks, which can decay further into leptons that are stable at detector scales.

While they do not have a lepton fraction that is as high as Models C and D, Models A and SVJ also have a relatively high lepton fraction. This is most likely because in Model A, the dark pions decay into charm quarks, and in Model SVJ the $\rho_{\mathrm{D}}^{\text{“0”}}$ can decay into charm or bottom quarks (among others). Both charm and bottom quarks can decay into leptons, which explain why these models have a non-negligible lepton fraction. Model B, on the other hand, has a very low lepton fraction, since it does not have any process that can produce a high number of leptons.

4.6.3 Dijet invariant mass

One way to discover models like Model B where the jets have no special features visible in experiments could be to look at the dijet invariant mass to try to find a bump at the mass of the Z' boson. The dijet invariant mass of the reconstruction level jets in the different dark jet models are shown in Figure 4.16.

In Models B and D, which have very low invisibility, we see a clear peak at 1500 GeV, which is the mass of the Z' boson in these models. The same is true for Model A where the invisibility is also quite low. This is similar to what we see in Figure 4.12a, but the peaks are a bit more spread out due to detector effects.

While these peaks look very clear in this figure, in reality, there will be a significant number of background events, which means that the peak would just be a small bump on the background. Similar bumps could appear in Standard Model events due to random fluctuations, so we would need a significant number of events and a careful statistical analysis to be able to discover this in real life.

In Model SVJ, and to a lesser extent in Model C, we see a peak that has a long tail at lower energies. This is because these are the models with high invisibility, and since invisible particles are not included in reconstruction level jets, their energy will be missing. These bumps could still be searched for, but would be even less clear than in Models A, B and D, so even harder to detect. However, as we saw in the previous sections there are other ways to discover these models, in particular lepton fraction for Model C and invisibility for Model SVJ.

In the models with a four jet topology (Figure 4.16b), we see a peak somewhere around 1000 GeV, however this peak is not clear at all. This is because unlike at the particle level (Figure 4.12b), we do not have access to the ancestors of the particles here, so we cannot use our particle level

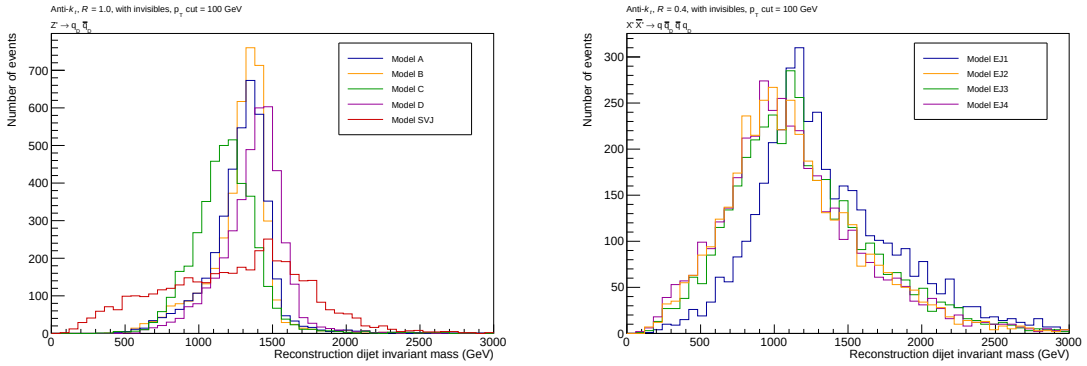

(a) Models A-D and SVJ

(b) Models EJ1-EJ4

Figure 4.16: Dijet invariant mass of the two leading reconstruction jets in different dark jet models.

definition to pair dark jets with Standard Model jets. So the best we can do at reconstruction level is to simply select the two leading jets, which is not always correct. This means that searching for bumps like this is not the correct way to try to detect models with a four jet topology.

4.6.4 Event shape observables

It is difficult to discover models with a four jet topology by looking at the dijet invariant mass since those models have four jets instead of two. However, there are other observables that allow to tell if an event is dijet-like or not. These are called *event shape observables*. Since the models with a four jet topology produce four jets, they should be non-dijet-like.

The two event shape observables that we will look at are the *thrust* $\mathcal{T}$ and the *sphericity* $\mathcal{S}$, defined as [31]

$$\mathcal{T} = \max_{\vec{n}} \frac{\sum_i |\vec{p}_i \cdot \vec{n}|}{\sum_i p_i} \qquad \mathcal{S} = \frac{\pi^2}{4} \min_{\vec{n}} \left(\frac{\sum_i ||\vec{p}_i \times \vec{n}||}{\sum_i p_i} \right)^2, \tag{4.9}$$

where $\vec{p}_i$ is the three-momentum of particle i, p_i is the norm of that three-momentum, and $\vec{n}$ is the normalized vector that maximizes the thrust or minimizes the sphericity, respectively.

Both event shape observables give a number between 0 and 1. Dijet-like events have a thrust close to 1 and a sphericity close to 0, whereas isotropic events have a thrust close to 0.5 and a sphericity close to 1 [32].

The thrust for the different dark jet models is plotted in Figure 4.18, and the sphericity is plotted in Figure 4.19. We see that for the models with a dijet topology, the thrust is rarely less than 0.8 and and is often very close to 1, whereas for models with a four jet topology the thrust can go all the way down to 0.6 and is almost never greater than 0.95. This is expected, since the Z' boson is expected to produce more dijet-like events than the X' boson. The sphericity also behaves as expected. For models with a dijet topology, the sphericity is often very close to zero and is rarely greater than 0.05, whereas for models with a four jet topology, the sphericity can go up to 0.15 and is rarely exactly zero.

However, there are also Standard Model processes that can produce non-dijet-like events, so just because events with a low thrust or high sphericity are observed does not necessarily mean that an X' boson has been discovered. One would have to compare the experimental data with theoretical predictions of how the Standard Model would behave to see if they are consistent.

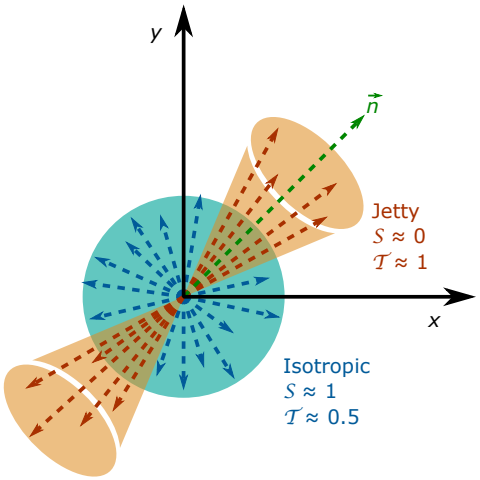

Figure 4.17: Illustration of how event shape observables behave with respect to different types of events. This figure shows the transverse plane, meaning that the beam axis is perpendicular to the plane of the figure. Source: [30]

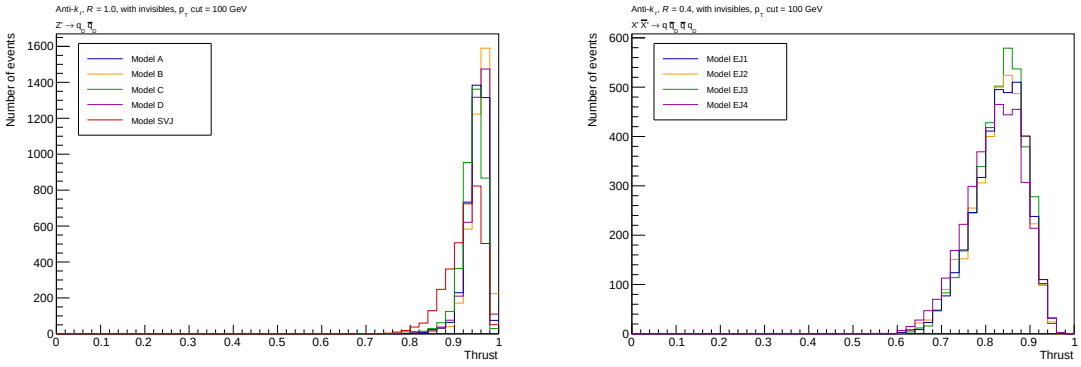

(a) Models A-D and SVJ

(b) Models EJ1-EJ4

Figure 4.18: Thrust in different dark jet models.

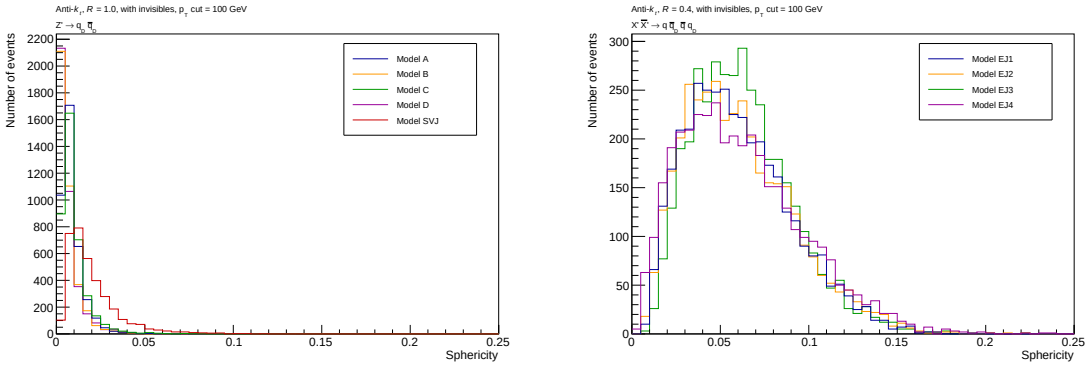

(a) Models A-D and SVJ

(b) Models EJ1-EJ4

Figure 4.19: Sphericity in different dark jet models.

5 Conclusion

In this thesis, we propose a technical definition of a dark jet, which is a hypothetical final state signature produced in certain dark sector models. It is intended to be applicable to any model that produces dark jets, and is implemented in the program Rivet, which is the standard interface between theoretical and experimental particle physicists.

The proposed baseline definition of a dark jet is a jet that has 80% of its p_{T} originating from dark particles. It has been validated on various different models to capture the expected parton level kinematics of each model. To target specific models, one can use properties of dark jets to create refined definitions. Two such properties are discussed in this thesis: invisibility and lepton fraction, which are defined as the p_{T} fractions carried by invisible particles and leptons respectively within the jet. For a specific analysis one can use such properties to adjust the definition of a dark jet, for example jets with a lepton fraction greater than a certain number in addition to the darkness requirement in the baseline definition.

Another jet property to consider, which has not been studied in this thesis, is displacement, which is the distance between the interaction point and the point from which the jet originates. This can be especially useful in models where dark mesons have a non-negligible lifetime without being stable at detector scales, such as the emerging jet models EJ1-EJ4 studied in this thesis.

While the 80% criterion used in the dark jet definition was found to be a good choice based on the studies performed in this thesis, this number is not set in stone. Future studies might prefer to adjust the criterion based on results from a larger and more varied set of models and generators. Future studies might also want to understand the theoretical robustness of this definition, for example if it is IR or UV safe if a dark gluon is radiated.

This definition can be used as a middle ground between the theoretical and experimental communities within particle physics. Theorists can use this definition to get a more realistic idea about the observable final state of a model, independent of any specific detector. Experimentalists can use it as a particle level target, and define dedicated experimental identification algorithms called "taggers" to be able to identify a specific type of dark jet, such as a dark jet with a high lepton fraction. Such tagging algorithms need to be derived for each experiment separately as it relies on the specific detector and object reconstruction.

Future experimental analyses can now target various dark jet final states with our proposed definition. They can for example set upper limits on the production rate of events with various final state topologies, based for instance on dark jet multiplicity, dijet invariant mass or jet properties. It will then be possible to immediately check future theoretical models to see if they produce more than the excluded amount of any of these final states, and if they do, they can be excluded. The Rivet code provided in association with this thesis [27] is easy to run and modify to check any specific (existing or future) theory prediction.

References

[1] Queen's University, *Evidence for Dark Matter* (accessed September 5th, 2022)
https://cdms.phy.queensu.ca/Public_Docs/DM_Intro.html

[2] A. H. G. Peter, *Dark Matter* (2012)
https://arxiv.org/pdf/1201.3942.pdf (arXiv:1201.3942)

[3] G. Jungman, M. Kamionkowski, and K. Griest, *Supersymmetric Dark Matter* (1995)
https://arxiv.org/pdf/hep-ph/9506380.pdf (arXiv:9506380 [hep-ph])

[4] R.D. Peccei, *The Strong CP Problem and Axions* (2006)
https://arxiv.org/pdf/hep-ph/0607268.pdf (arXiv:0607268 [hep-ph])

[5] G. Albouy et. al., *Theory, phenomenology, and experimental avenues for dark showers: a Snowmass 2021 report* (2021)
https://arxiv.org/pdf/2203.09503.pdf (arXiv:2203.09503)

[6] S. Bethke, G. Dissertori and G.P. Salam, *Quantum Chromodynamics* (2017)
https://pdg.lbl.gov/2018/reviews/rpp2018-rev-qcd.pdf

[7] F. Gross et. al., *50 Years of Quantum Chromodynamics* (2022)
https://arxiv.org/ftp/arxiv/papers/2212/2212.11107.pdf (arXiv:2212.11107)

[8] C. Amsler et. al. (Particle Data Group), *PL B667*, 1 (2008)
https://pdg.lbl.gov/2008/listings/m018.pdf

[9] S. Renner and P. Schwaller, *A flavoured dark sector* (2018)
https://arxiv.org/pdf/1803.08080.pdf (arXiv:1803.08080)

[10] M. Park and M. Zhang, *Tagging a jet from a dark sector with Jet-substructures at colliders* (2020)
https://arxiv.org/pdf/1712.09279.pdf (arXiv:1712.09279)

[11] E. Bernreuther et. al., *Casting a graph net to catch dark showers* (2021)
https://arxiv.org/pdf/2006.08639.pdf (arXiv:2006.08639)

[12] O. Buchmueller, M. J. Dolan, S. A. Malika and C. McCabe, *Characterising dark matter searches at colliders and direct detection experiments: Vector mediators* (2015)
https://arxiv.org/pdf/1407.8257.pdf (arXiv:1407.8257)

[13] S. Knapen, J. Shelton and D. Xu, *Perturbative benchmark models for a dark shower search program* (2022)
https://arxiv.org/pdf/2103.01238.pdf (arXiv:2103.01238)

[14] P. Schwaller, D. Stolarski and A. Weiler, *Emerging Jets* (2015)
https://arxiv.org/pdf/1502.05409.pdf (arXiv:1502.05409)

[15] T. Cohen et. al., *LHC Searches for Dark Sector Showers* (2017)
https://arxiv.org/pdf/1707.05326.pdf (arXiv:1707.05326)

[16] C. Cazzaniga and A. de Cosa, *Leptons lurking in semi-visible jets at the LHC* (2022)
https://arxiv.org/pdf/2206.03909.pdf (arXiv:2206.03909)

[17] The ATLAS Collaboration, *The ATLAS Experiment at the CERN Large Hadron Collider* (2008)
https://iopscience.iop.org/article/10.1088/1748-0221/3/08/S08003/pdf
(doi:10.1088/1748-0221/3/08/S08003)

[18] The ATLAS Collaboration, *ATLAS Fact Sheets* (accessed March 25th, 2023)
https://atlas.cern/Resources/Fact-sheets

[19] T. Sjöstrand et. al., *An Introduction to PYTHIA 8.2* (2014)
https://arxiv.org/pdf/1410.3012.pdf (arXiv:1410.3012)

[20] CERN, *The Large Hadron Collider* (accessed March 25th, 2023)
https://home.web.cern.ch/science/accelerators/large-hadron-collider

[21] M. Dobbs and J. B. Hansen, *The HepMC C++ Monte Carlo Event Record for High Energy Physics* (2000)
http://cds.cern.ch/record/684090/files/soft-2000-001.pdf (ATL-SOFT-2000-001)

[22] G. Duckeck et. al., *ATLAS Computing: Technical Design Report* (2005)
http://cds.cern.ch/record/837738/files/lhcc-2005-022.pdf
(ATLAS-TDR-17; CERN-LHCC-2005-022)

[23] C. Bierlich et. al., *Robust Independent Validation of Experiment and Theory: Rivet version 3* (2020)
https://arxiv.org/pdf/1912.05451.pdf (arXiv:1912.05451)

[24] R. Brun and F. Rademakers, *ROOT - An Object Oriented Data Analysis Framework*, Proceedings AIHENP'96 Workshop, Lausanne, Sep. 1996, Nucl. Inst. & Meth. in Phys. Res. A 389 (1997) 81-86. See also "ROOT" [software], Release 6.26/10, 16/11/2022
https://root.cern/

[25] M. Cacciari, G. P. Salam and G. Soyez, *FastJet user manual* (2011)
https://arxiv.org/pdf/1111.6097.pdf (arXiv:1111.6097)

[26] L. Garren et. al., *Monte Carlo particle numbering scheme* (2006)
https://pdg.lbl.gov/2007/reviews/montecarlorpp.pdf

[27] G. Lindberg, *Particle Level Dark Jet* (2023)
https://github.com/DarkJets-hep/ParticleLevelDarkJet

[28] The ATLAS Collaboration, *Performance of jet substructure techniques for large-R jets in proton–proton collisions at* $\sqrt{s} = 7\,\text{TeV}$ *using the ATLAS detector* (2013)
https://arxiv.org/pdf/1306.4945.pdf (arXiv:1306.4945)

[29] N. K. Hemme, *Studies of Dark Showers for Present and Future Colliders* (2022)
https://lup.lub.lu.se/luur/download?func=downloadFile&recordOId=9093940
(LUP:9093940)

[30] S. Prasad et. al., *Event topology and global observables in heavy-ion collisions at the Large Hadron Collider* (2022)
https://www.nature.com/articles/s41598-022-07547-z.pdf
(doi:10.1038/s41598-022-07547-z)

[31] The ATLAS Collaboration, *Measurement of event-shape observables in* $Z \to \ell^+\ell^-$ *events in pp collisions at* $\sqrt{s} = 7\,\text{TeV}$ *with the ATLAS detector at the LHC* (2016)
https://arxiv.org/pdf/1602.08980.pdf (arXiv:1602.08980)

[32] M. Botje, *Quantum Chromo Dynamics: Soft and Collinear Singularities* (2013)
https://www.nikhef.nl/~h24/qcdcourse/section-7.pdf